2008

Final report: Phase stability and segregation in Alloy 22 base metal and weldments

Jeffrey LaCombe
University of Nevada, Reno, lacomj@unr.edu

Final Report:
Task: ORD-FY04-015
Phase Stability and Segregation in Alloy 22 Base Metal and Weldments

J.C. LaCombe[1]

Chemical and Metallurgical Engineering
University of Nevada, Reno,
Reno, NV 89557 USA

Project Background

At the outset of this project, the design of the waste disposal containers relied heavily on encasement in a multi-layered container, featuring a corrosion barrier of Alloy 22, a Ni-Cr-Mo-W based alloy with excellent corrosion resistance over a wide range of conditions. The fundamental concern from the perspective of the Yucca Mountain Project, however, was the inherent uncertainty in the (very) long-term stability of the base metal and welds. Should the properties of the selected materials change over the long service life of the waste packages, it was conceivable that the desired performance characteristics (such as corrosion resistance) would become compromised, leading to premature failure of the system. To address this, we studied aspects of the phase stability and solute segregation characteristics of Alloy 22 base metal, and the manner in which these affected corrosion resistance. This work was conducted as an independent validation, to add to confidence in the extrapolated behavior of the container materials over time periods that are not feasibly tested in a laboratory.

Ni base alloys with 16-22% chromium and 9-16% molybdenum are commonly used for higher corrosion resistance applications. Alloy-22 (UNS N06022), a Ni-Cr-Mo-W alloy, is the current reference material for construction of the outer wall of nuclear waste containers [1, 2, 3, 4] to be used by the Yucca Mountain Project. The nominal composition of Alloy-22 and the compositions of some of the reported phases seen in this alloy system are listed in Table 1.

Even though Alloy-22 in wrought form is considered to have good phase stability at the operating temperatures $< 200\,^{\circ}\mathrm{C}$ of the repository, exposure to elevated temperatures during the fabrication processes (such as welding and stress relieving) could cause alteration of microstructure and associated deterioration of mechanical and corrosion properties. Welding causes microstructural changes in Alloy-22, such as formation of dendrites in the weld metal, segregation of Mo and W in the interdendritic regions, formation of topologically close packed phases both in the weld metal and the heat affected zone (HAZ), and possibly precipitation

[1]To whom correspondence should be addressed: e-mail lacomj@unr.edu.

Phase	Ni	Mo	Cr	W	Fe	Co
Nominal	56.96	13.43	21.22	3.29	3.17	0.84
γ (matrix)	58.5	12.7	21.6	2.9	3.4	0.9
μ	33.1	38.7	19.3	6.3	2.1	0.6
p	32.6	37.4	21.7	5.3	2.2	0.9
σ	34.5	34.9	23.4	4.2	2.2	0.9

Table 1: Compositions of various phases in Alloy-22 and related alloys

of long range ordered phases[3, 5, 6, 7]. Formation of such secondary phases could make the material susceptible to intergranular corrosion and/or reduce strength and ductility [8, 9, 10]. Whereas the equilibrium solidification phase of Alloy-22 is the austenitic γ phase (which can be obtained by quenching), at lower temperatures, secondary phases such as μ are thermodynamically stable at the Alloy-22 composition. Figure 1 (adapted from [11]) illustrates that at 850 °C, the equilibrium phases to be expected include $\mu + \gamma$. At still lower temperatures, the $\gamma \Leftrightarrow \mu + \gamma$ boundary is expected to move even closer to the Ni corner of the diagram (see dashed line in the figure). This may make the alloy potentially susceptible to phase separation at lower temperatures.

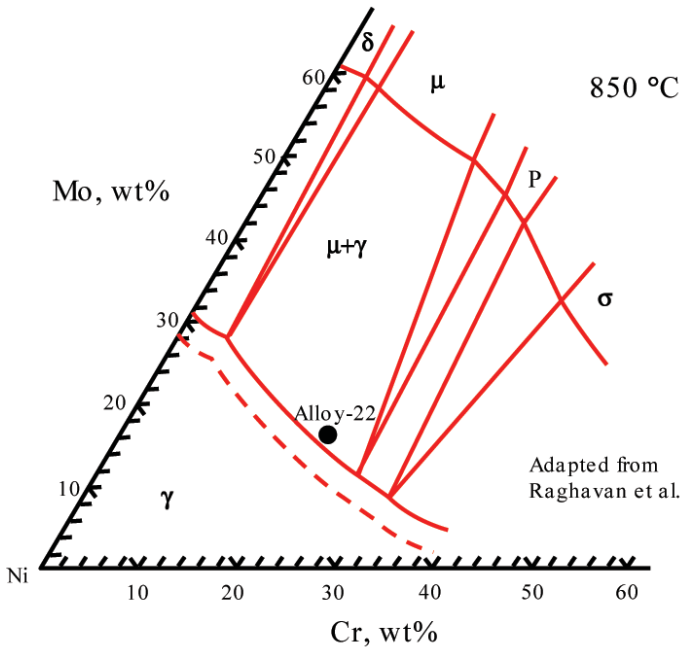

Figure 1: Isothermal section of Cr-Ni-Mo alloy phase diagram at 850 °C

In low carbon Ni-Cr-Mo alloys, sensitization has been reported to occur mainly because of the precipitation of topologically close packed (TCP) phases like μ and p [2, 3, 4, 5, 6, 7]. Increased corrosion rates of aged Ni-Cr-Mo-W alloys were observed because of this sensitized microstructure [10]. The sensitization of Mo-rich nickel base alloys is found to be different from the sensitization of common austenitic stainless steels and other Ni-Cr alloys such as

Inconel 600. Sensitization of austenitic stainless steel resulted in depletion of chromium adjacent to the chromium rich $M_{23}C_6$ carbides [12, 13]. In the Ni-Cr-Mo alloys, sensitization resulted in depletion of molybdenum near the TCP or M_6C precipitates [10, 14]. When the sensitized Ni-Cr-Mo alloys were exposed to a reductive environment the Mo depleted regions were preferentially attacked and in an oxidizing environment the TCP phases themselves were dissolved, giving rise to the corrosion rate [14]. Raghavan *et al.* [11] and Cieslak *et al.* [5, 6, 7] observed the TCP phases containing only the nominal chromium as that of the bulk chemistry. Whereas, Hodge [14, 15] reported that the μ phase was enriched with Cr and the suggested phase was (Ni, Fe, Co)$_3$(W, MO, Cr)$_2$. This issue is not fully resolved as of yet. There are no reports available on the depletion profiles of aged Alloy-22. Depletion of alloying elements in the vicinity of secondary phase precipitates will impair the corrosion resistance of the alloy. Therefore, it is imperative to develop an understanding of how the microstructure changes during fabrication or exposure to service conditions so that the integrity of the waste package container can be ensured.

The three principal efforts of this project were:

Subtask 1: Microstructural Characterization of Phase Stability and Variability in Alloy 22 Develop an improved understanding of Alloy 22 and the extent to which compositional and microstructural variations are present in otherwise nominal as-procured material.

Subtask 2: Electrochemical Methods to Detect Susceptibility of Alloy 22 to Localized Corrosion Study the influence that compositional and microstructural variations have on the corrosion performance of Alloy 22.

Subtask 3: Multicomponent Diffusivity of Alloy 22 Preliminary investigation of the role of diffusion in Alloy-22 at repository temperatures (scoping study).

Subtask 1: Microstructure

The principal goal of Subtask 1 was to develop an improved understanding of Alloy 22 and the extent to which compositional and microstructural variations are present in otherwise nominal as-procured material. This involved the following questions

1. Characterize the as-fabricated Alloy-22 base metal.
2. Characterize Alloy-22 welds (goal eliminated mid-project)
3. Long-term metallurgical stability: Cr-Mo depletion and Long Range Ordering
4. Segregation of sulfur and phosphorous.

This research has studied the microstructural variabilities in Alloy 22 using various characterization techniques. Light optical, scanning electron, and transmission electron microscopy techniques were used to metallurgically examine the characteristics of secondary phases. The conclusions are summarized, as follows:

1. Light optical microscope micrographs exhibited expected precipitate formation at sensitizing conditions and dissolution at solutionizing conditions, as predicted by the equivalent element ternary Ni-Cr-Mo phase diagram and observations from other researchers. Increases of precipitation with temperature were not intensely observed.

2. Scanning electron microscopy with energy-dispersive X-ray spectroscopy confirmed the depletion of nickel, chromium, and tungsten along with segregation of molybdenum, within a grain boundary, but not accurate enough to differentiate the type of phase. These material compositional variations give some confidence on the presence of precipitates but limited since using etched specimens.

3. Transmission electron microscopy with energy-dispersive X-ray spectroscopy results did not match previous works exactly, complexity of Alloy 22 element composition is speculated to be at fault, but did closely follow the characteristics of the μ phase. This result was expected from the ternary phase diagrams for Ni-Cr-Mo and from other researchers.

4. Microhardness measurements indicated no significant changes with increasing sensitizing durations, only a 10% hardness increase was observed with increasing sensitizing temperatures. Macrohardness measurements displayed less variability, compared to microhardness, and did increase with higher temperatures and sensitizing durations. Since the sensitizing temperatures were not in range of long-range ordering formations, the only contributing factors to hardness increase are with carbides and secondary phases. The hardness values agree with previous works. Large deviations from the microhardness testing are due to the grain-to-grain variability and are not sufficient to measure precipitate formation as functions of time and temperature.

5. Grain size measurements were conducted for Alloy 22 specimens in the as-received, sensitized, and solutionized conditions. Comparisons for each category showed trends with unpredictable behaviors caused by either the ambiguous duplex microstructure of the alloy, or the large confidence intervals of the data sets. Grain growth kinetics could not be adequately confirmed.

6. Phase fraction analysis proved to be successful using backscattered SEM micrographs and Scentis software, despite only using one specimen. Resulting data is not sufficient for precipitate growth and dissolution conclusions.

7. All measurements included moderately high standard deviations due to the influence of data outliers, which is expected in small data sets. Results have shown that an increase in data points can lead to more statistically significant results. Specific measurement techniques have been developed in this research and are expected to continue with lager data sets in future works.

8. The long-term metallurgical stability of Alloy 22 is dependent on the dissolution of secondary phases, since the increase of temperature and time during sensitizing heat treatments has been shown to influence precipitation and accumulate in the grain

boundaries leading to saturation in the bulk material. Limitations must be considered for the control of energies introduced into the material during production or fabrication.

Subtask 2: Corrosion

Goals

The main mode of corrosion that may occur at the repository site was examined here. Alloy-22 (C-22) is a versatile nickel-chromium-molybdenum-tungsten alloy with good overall corrosion resistance. It is claimed that C-22 alloy has outstanding resistance to pitting, crevice corrosion, and stress corrosion cracking. Intergranular corrosion and exposure of Alloy-22 to moderately elevated temperatures may potentially lead to diminished corrosion resistance an issue that we examine here. The intergranular corrosion resistance of Alloy-22 after various heat treatments on both mill annealed and welded samples was studied using ASTM G28 tests. We attempted to corroborate these results using suitable methods such as double-loop electrochemical potentiokinetic reactivation (EPR) tests, as well as material characterization techniques including optical microscopy, scanning electron microscopy (SEM), and energy dispersive spectrometry (EDS). The samples were tested using electrochemical potentiokinetic reactivation (EPR) tests in solutions that were developed specifically so as to check for chromium and molybdenum depletion.

Alloy 22 is considered to be less susceptible to Localized corrosion (LC), due to the additions of Mo and W, both of which are believed to stabilize the passive film at very low pH. The oxides of these elements are believed to be very insoluble at low pH, as a result of which Alloy 22 is believed to exhibit relatively high thresholds for localized attack [18]. Alloy-22 (UNS N06022) is said to rely on the stability of a thin chromium oxide film for protection against corrosion [19]. Alloy 22 was supposedly designed to resist the most aggressive industrial applications, offering a low general corrosion rate under both oxidizing and reducing conditions [20]. It is believed that Chromium exerts its beneficial effect in the alloy under oxidizing and acidic conditions, under reducing conditions the most beneficial alloying elements are molybdenum and tungsten which offer a low exchange current density for hydrogen discharge. Alloy 22 is believed to be an excellent alternative to austenitic stainless steels that may fail by pitting corrosion or stress corrosion cracking (SCC) in hot chloride containing solutions due to its balanced content in chromium, molybdenum and tungsten [21, 22].

The principal goal of Subtask 2 was to study the influence that compositional and microstructural variations have on the localized corrosion performance of Alloy 22. This was divided into smaller goals.

1. Develop an EPR test solution and Cr depletion test procedure
2. Develop an electrochemical test solution and Mo segregation test procedure
3. Study the effect of precipitation of secondary phases on the corrosion resistance of Alloy-22

Results: Chemical Weight Loss Tests

ASTM G 28 Chemical Weight Loss Test Results Discussion

The test results were consistent with the results that were reported by Gorhe *et.al* [23]. The sample that was sensitized at 650 °C for 60 minutes showed a corrosion rate of 22.83 mpy after the ASTM-G-28-A test. Gorhe *et.al* [23] reported a corrosion rate of 21.98 mpy for an Alloy 22 sample that was given a similar heat treatment after a similar test. Another sample that was sensitized at 750 °C for 60 minutes showed a corrosion rate of 27.29 mpy after the ASTM-G-28-A test close to the corrosion rate of 30.57 mpy obtained by Gorhe *et.al* [23]. Alloy 22 samples that were sensitized at 700 °C for about 6000 minutes showed a corrosion rate of 151.98 mpy after the ASTM-G-28-A test as reported by Gorhe *et.al* [23]. While our tests on a sample given the similar heat treatment for the same time showed a lesser corrosion rate of 46.56 mpy. In the ASTM-G-28-B tests that were done on Alloy 22 samples sensitized at 650 °C, 70 °C for 60 minutes showed corrosion rates of 40.51mpy, 2070.59 mpy after the ASTM-G-28-B tests respectively. Gorhe *et.al* [23] reported lower corrosion rates of 5.2 mpy, 47.64 mpy after the ASTM-G-28-B tests for similar samples respectively. The samples that were sensitized at 650 °C and 750 °C for about 6000 minutes showed corrosion rates of 3179.58 mpy, 3504.72 mpy after the ASTM-G-28-B tests in our work which were similar to the results obtained by Gorhe *et.al* [23] which are 3398.82 mpy, 4002.76 mpy respectively on samples given the similar heat treatments after the similar test.

Mill Annealed Condition

The samples in the mill-annealed condition showed corrosion rates ranging from 5.11 mpy to 29.52 mpy for different samples after the ASTM-G-28-A test. The ASTM-G-28-B test results showed corrosion rates ranging from 3.96 mpy to 26.55 mpy for various mill-annealed Alloy-22 samples.

Sensitized Condition

The ASTM-G-28-A test results for the Alloy 22 samples after being sensitized at various temperatures for 60 minutes showed a clear trend of increase in the corrosion rate with increase in the temperature of sensitization from 650 °C all the way to 750 °C. The corrosion rate values after the ASTM-G-28-A test for the samples sensitized for 60 minutes increased from 18.4 mpy from an Alloy 22 sample sensitized at 650 °C to 27.29 mpy for an Alloy 22 sample sensitized at 750 °C. Although ASTM-G-28-A test results for samples sensitized for 600 minutes showed corrosion rates of 26.26 mpy at a sensitization temperature of 650 °C and a corrosion rate of 23.96 mpy at a sensitization temperature of 750 °C. The corrosion rate values after the ASTM-G-28-A test for the samples sensitized for 60 minutes increased from 18.4 mpy from an Alloy 22 sample sensitized at 650 °C to 27.29 mpy for an Alloy 22 sample sensitized at 750 °C. The corrosion rate values after the ASTM-G-28-A test for the samples sensitized for 6000 minutes increased from 46.56 mpy from an Alloy 22 sample sensitized at 700 °C to 91.58 mpy for an Alloy 22 sample sensitized at 850 °C which again shoed the relevance of increase in the temperature of sensitization on the corrosion rates. There wasnt

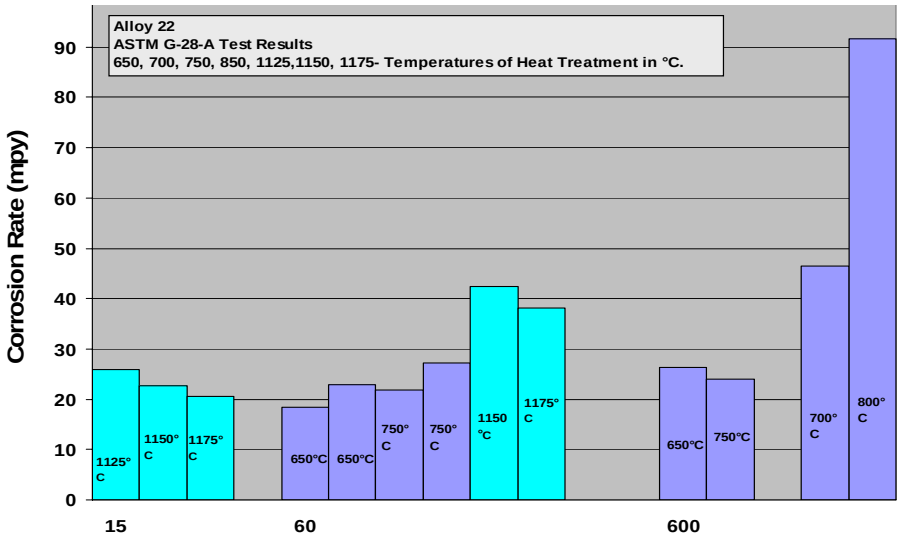

Figure 2: ASTM-G28A Chemical Weight Loss Test Results

such a clear effect of the time of sensitization on the corrosion rate though the average corrosion rate of the various samples done for every segment of the time of sensitization clearly increased in the direction of the larger times of sensitization. The ASTM-G-28-A test results for the various sensitized samples/batches obtained from different manufacturers showed almost similar results. For example the ASTM-G-28-A test results for two different Alloy 22 samples, both sensitized at 750 °C for 60 minutes showed corrosion rates of 18.4, 21.84 mpy respectively. The ASTM-G-28-B test results for the Alloy 22 samples after being sensitized at various temperatures for 60 minutes showed a clear trend of increase in the corrosion rate with increase in the temperature of sensitization from 650 °C all the way to 750 °C. The corrosion rate values after the ASTM-G-28-A test for the samples sensitized for 60 minutes increased from 40.51 mpy from an Alloy 22 sample sensitized at 650 °C to 3504.72 mpy for an Alloy 22 sample sensitized at 750 °C. The corrosion rate value after the ASTM-G-28-B test for the samples sensitized for 60000 minutes showed a corrosion rate of 3023.71 mpy for an Alloy 22 sample sensitized at 850 °C which again showed the relevance of increase in the temperature of sensitization on the corrosion rates. There was also a clear effect of the time of sensitization on the corrosion rate with the average corrosion rate of the various samples done for every segment of the time of sensitization clearly increasing in the direction of the larger times of sensitization. The ASTM-G-28-B test results for the various sensitized samples/batches obtained from different manufacturers showed almost similar results. For example the ASTM-G-28-B test results for three different Alloy 22 samples, all sensitized at 750 °C for 6000 minutes showed corrosion rates of 2978.73, 2774.09, 3504.72 mpy respectively. In general the average corrosion rates of sensitized samples of Alloy 22 were about 100 times higher for the ASTM-G-28-B test compared to the ASTM-G-28-A tests.

The results of the ASTM-G28A tests of sensitized samples are summarized in Figure 2. Similarly, the results of the ASTM-G28B sensitized tests are summarized in Figure 3.

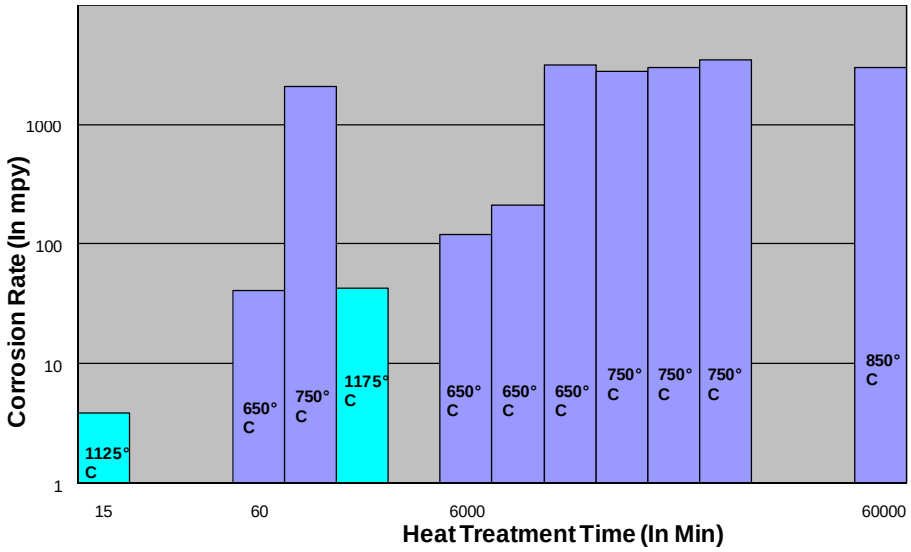

Figure 3: ASTM-G28B Chemical Weight Loss Test Results

Solutionized Condition

The ASTM-G-28-A test results for the various Alloy 22 samples that were given solution heat treatment showed a clear trend of decreasing corrosion rates with increase in temperature. The corrosion rates for three different Alloy 22 samples that were solutionized for 15 minutes at temperatures of 1125 °C, 1150 °C, 1175 °C showed corrosion rates of 25.93, 22.76, 20.64 mpy respectively. The average corrosion rate though definitely increased with increase in the time of solution treatment in minutes. Again at 60 minutes of solution treatment Alloy 22 showed higher corrosion rate for solution treatment at 1150 °C compared to the solution treatment at 1175 °C. The solution heat treatment showed corrosion rates that peaked at lower temperatures for higher times of heat treatment compared to the sensitization treatment that showed corrosion rates which peaked at both higher temperatures and times of sensitizations. The maximum corrosion rates though were the highest in sensitized samples and the average corrosion rate was also higher in sensitized samples. The ASTM-G-28-B test results for the various Alloy 22 samples that were given solution heat treatment showed a higher corrosion rate for a sample with increase in the time of solution treatment as well as the temperature. The solution heat treatment showed corrosion rates that peaked at higher temperatures for higher times of heat treatment just like the sensitization treatment that showed corrosion rates which peaked at both higher temperatures and times of sensitizations. The maximum corrosion rates though were the highest in sensitized samples and the average corrosion rate was also higher in sensitized samples for the ASTM-G-28-B tests.

A comparison of sensitized and solutionized ASTM-G28A test results is shown in Figure 4, and for ASTM-G28B in Figure 5. Figures 6 (ASTM-G28A) and 7(ASTM-G28B) show variations in chemical weight loss for several manufacturers.

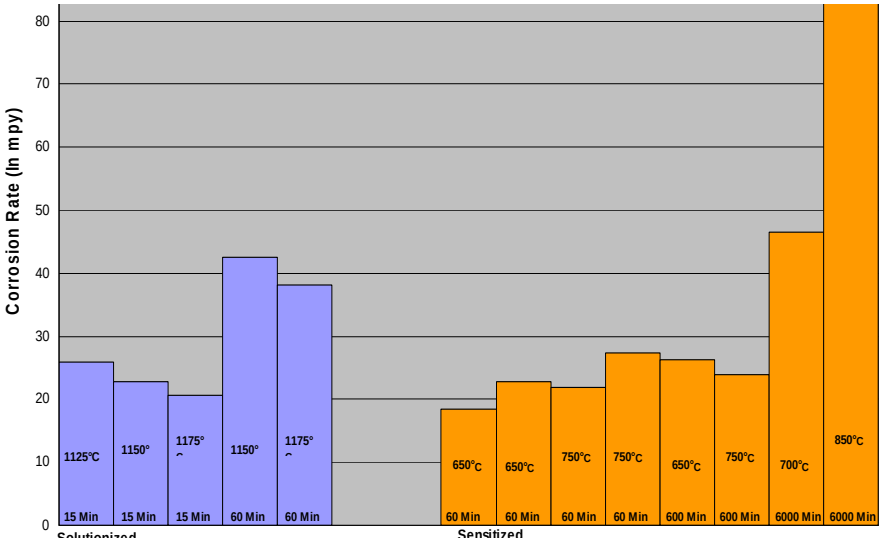

Figure 4: ASTM-G-28-A Test Results for Various Sensitized and Solutionized Samples.

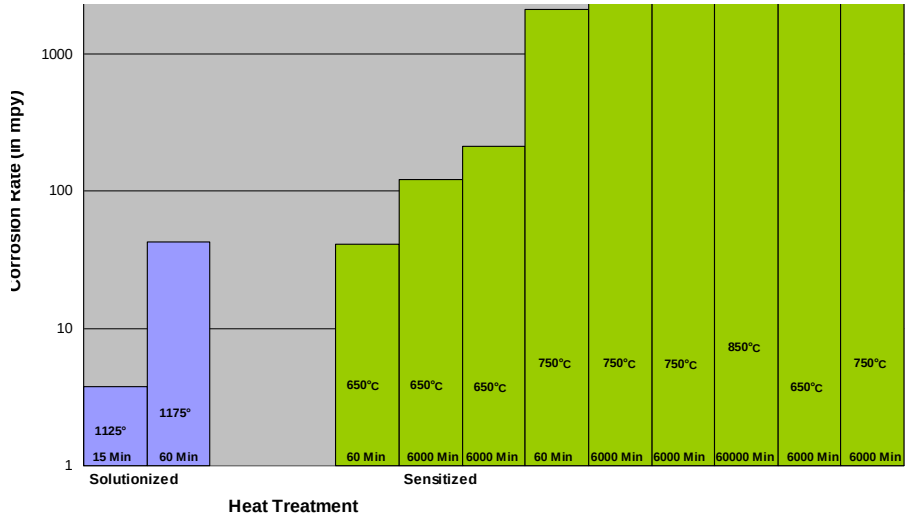

Figure 5: ASTM-G-28-B Test Results for Various Sensitized and Solutionized Samples.

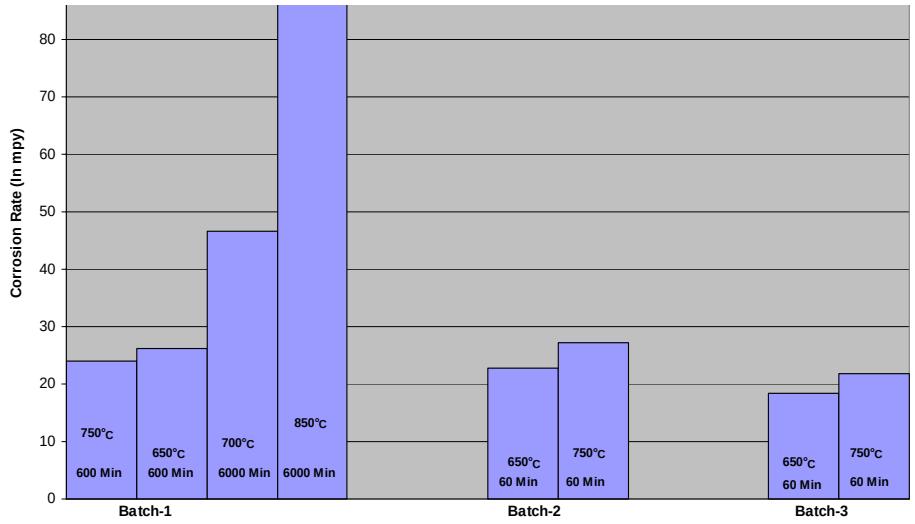

Figure 6: ASTM-G-28-A Test Results for Sensitized Samples from Various Batches obtained from Various Manufacturers.

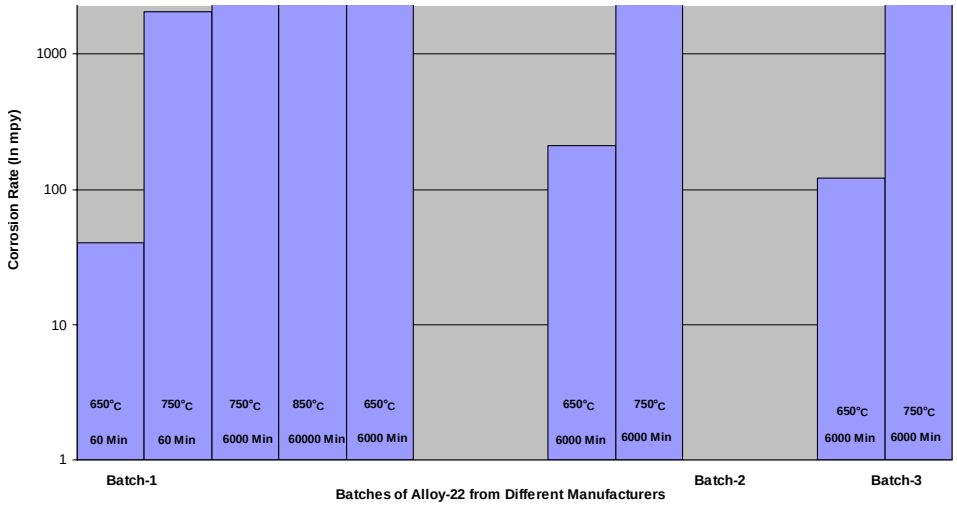

Figure 7: ASTM-G-28-B Test Results for Sensitized Samples from Various Batches obtained from Various Manufacturers.

Results: EPR Tests

Double-Loop EPR Tests in 5 Wt% NaCl Solution (pH-7) at a Temperature of 30 °C.

Two of the mill-annealed samples showed that the risk of localized corrosion is extremely low. Even the general corrosion is not predicted, the general corrosion rate may be at most a contamination rate. One mill-annealed sample showed suspected risk of localized corrosion in the form of crevice corrosion which might be present in areas such as close proximity of surfaces, areas under deposits, and metal- silicone O-ring interfaces may be prone to such attack. But such assumptions can only be conformed using longer term immersion tests with, for example, artificial crevice formers which are implied to confirm crevice corrosion prediction.

In the sensitized samples the sample that was sensitized at 650 C for 60 minutes, sensitized at 700C for 600 minutes, sensitized at 700 C for 6000 minutes, 750C for 6000 minutes, 700C for 6000 minutes (batch-2) showed that no attack is being predicted. The risk of localized corrosion was extremely low so as to call it negligible. Even general corrosion was not predicted at all in these samples. The samples that were sensitized at 650C for 600 minutes, 750C for 60 minutes showed that the risk of localized corrosion in the form of crevice corrosion in close proximity of surfaces such as metal-O-ring interfaces etc. might be there. Though longer term immersion tests with, for example, artificial crevice formers are implied to confirm crevice corrosion prediction.

In the solutionized samples the one that was solutionized at 1150C for 30 minutes, and the one that was solutionized at 1125C for 30 minutes showed predictions of crevice corrosion in close proximity of surfaces such as metal-O-ring interfaces etc. Pitting may occur in non-occluded areas. As again, it needs to be conformed by longer term immersion tests with, for example, artificial crevice formers are implied to confirm crevice corrosion prediction. The sample that was solutionized at 1125C for 30 minutes showed a slight activation peak which was seen at a current density of 280.7 μA and a reactivation peak at 163.7 μA. The ratio of Ir to Ia was about 0.6. Sensitization at the grain boundaries to a certain extent is being suspected. When the Alloy 22 sample was solutionized at 1175C for 120 minutes traces of general corrosion was suspected. But this needs to be conformed by coupon immersion testing, electrochemical impedance spectroscopy, or polarization resistance methods which are suggested to confirm predictions, since corrosion rates cannot be easily estimated from polarization scans. An example DL-EPR test is depicted in the plot in Figure 8.

Double-Loop EPR Tests in 10 Wt% NaCl Solution (pH-7) at a Temperature of 60 °C.

As expected all the mill-annealed samples showed that the risk of localized corrosion is extremely low and no attack was predicted. Even the general corrosion is not predicted, the general corrosion rate may be at most a contamination rate.

The samples that were tested including the ones sensitized at 700 C for 600 minutes, sensitized at 750 C for 60 minutes, sensitized at 750 C for 6000 minutes showed risk of localized corrosion is extremely low almost that no attack was being predicted. Though

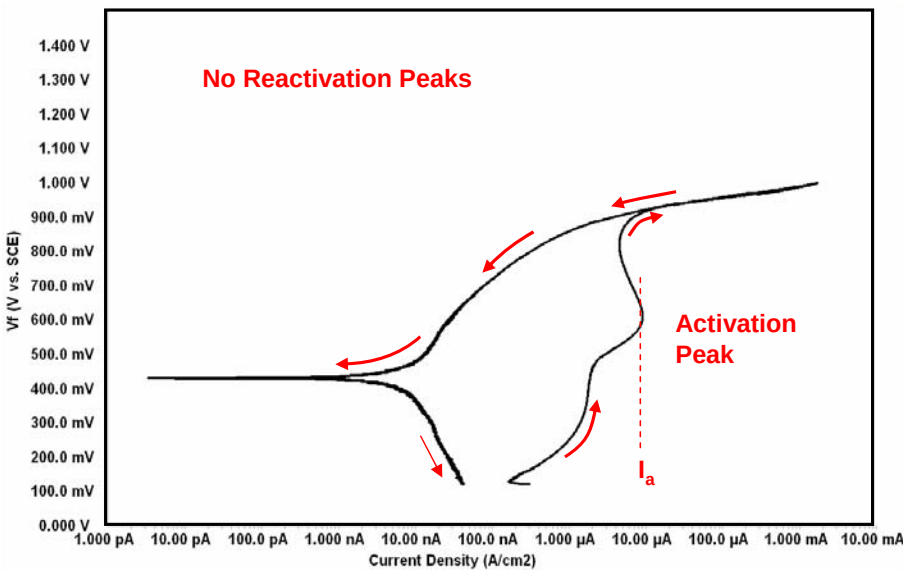

Figure 8: Example DL-EPR Plot: Mill Annealed, 1M H2SO4 + 0.5M NaCl + 0.01 M KSCN, at 30 °C (test for Cr-depletion)

general corrosion is not predicted, the general corrosion rate may be at most a contamination rate. If metal ion contamination is important, corrosion rate should be checked by alternative experimental methods.

The samples like the one sensitized at 650 C for 60 minutes, sensitized at 650 C for 600 minutes, sensitized at 700 C for 6000 minutes showed that localized corrosion in the form of crevice corrosion is present. Such areas as close proximity of surfaces, areas under deposits, and metal-O-ring, metal-PTFE gasket interfaces may be prone to such attack. Pitting may occur in non-occluded areas. Longer term immersion tests with, for example, artificial crevice formers, are definitely required to further consolidate this suspicion.

All the solutionized samples including the one that was solutionized at 1150C for 30 minutes, the one that was solutionized at 1125C for 30 minutes, and the one solutionized at 1175 C for 120 minutes showed predictions of crevice corrosion in close proximity of surfaces such as metal-O-ring interfaces etc. pitting may occur in non-occluded areas. As again, it needs to be conformed by longer term immersion tests with, for example, artificial crevice formers are implied to confirm crevice corrosion prediction. General corrosion is not predicted in all the cases.

Double-Loop EPR Tests in 10 Wt% NaCl Solution (pH 1-2) at a Temperature of 60 °C**.**

All the mill annealed samples showed that the risk of localized corrosion was extremely low. Though general corrosion is not predicted, the general corrosion rate may be at most a contamination rate. There was slight risk of localized corrosion in the form of crevice corrosion in one of the samples. It was suspected in close proximity of surfaces, areas under deposits, and metal-PTFE gasket interfaces. Pitting might be observed in non-occluded areas. Longer term immersion tests with, for example, artificial crevice formers, can be used so as to further substantiate the results. An activation peak measuring a current density of 3.29 ?A was seen in this sample.

The samples like the one sensitized at 650 C for 600 minutes, sensitized at 750 C for 600 minutes, sensitized at 700 C for 6000 minutes, sensitized at 750 C for 600 minutes showed that localized corrosion in the form of crevice corrosion is present. Such areas as close proximity of surfaces, areas under deposits, and metal-O-ring, metal-PTFE gasket interfaces may be prone to such attack. Pitting may occur in non-occluded areas. Longer term immersion tests with, for example, artificial crevice formers, are definitely required to further consolidate this suspicion. No general corrosion was predicted in these samples. A slight activation peak was seen at a current density of 1.48 μA in the forward direction in the sample that was sensitized at 700 C for 6000 minutes. The sample sensitized at 700 C for 600 minutes showed no risk of localized corrosion at all. The sample sensitized at 750 C for 60 minutes showed suspected measurable general corrosion rate. This needs to be substantiated using alternative measurements of corrosion rate by coupon immersion testing, electrochemical impedance spectroscopy, or polarization resistance methods which are used to confirm predictions. In the Alloy 22 sample that was sensitized at 750 C for 6000minutes an activation peak at the current density Ia of 20.25 μA was seen. A reactivation peak was also seen in the reverse direction at a current density Ir of 3.281 μA. The ratio of Ir to Ia is about 0.17 indicating sensitization at the grain boundary.

The solutionized samples that was solutionized at 1150C for 30 minutes showed extremely low risk of localized corrosion and no general corrosion was predicted., the one that was solutionized at 1125C for 30 minutes although showed borderline crevice corrosion which might occur at the metal-O-ring interface, and the one solutionized at 1175 C for 120 minutes showed predictions of crevice corrosion in close proximity of surfaces such as metal-O-ring interfaces etc. pitting may occur in non-occluded areas. As again, it needs to be conformed by longer term immersion tests with, for example, artificial crevice formers are implied to confirm crevice corrosion prediction. General corrosion is not predicted in all the cases. No general corrosion was predicted even in this case.

Double-Loop EPR Tests in 10 Wt% NaCl Solution (pH 13-14) at a Temperature of 60 °C**.**

Two of the mill annealed samples showed that the risk of localized corrosion was extremely low. Though general corrosion is not predicted in one of these samples, there is a suspected general corrosion rate that may be predicted to be measurable in the other one. Alternative measurements of corrosion rate like coupon immersion testing, electrochemical impedance spectroscopy, or polarization resistance methods are suggested to confirm these predictions since corrosion rates cannot be easily estimated from polarization scans.

A slight activation peak was seen measuring a current density Ia of about 54.97 μA in this sample. A slight activation peak was seen measuring a current density Ia of about 6.12 μA was seen in the other sample. There was borderline risk of localized corrosion in the form of crevice corrosion in the third sample. It was suspected in close proximity of surfaces, areas under deposits, and metal-PTFE gasket interfaces Longer term immersion tests with, for example, artificial crevice formers, can be used so as to further substantiate the results. A fourth sample showed no signs of neither localized corrosion nor general corrosion.

The samples like the one sensitized at 650 C for 60 minutes, sensitized at 650 C for 600

minutes, sensitized at 700 C for 600 minutes that the risk of localized corrosion is extremely low to the extent that it is almost negligible. Though general corrosion is not predicted, the general corrosion rate may be at most a contamination rate. If metal ion contamination is important, corrosion rate should be checked by alternative experimental methods.

The sample that was sensitized at 700 C for 600 minutes showed suspicions of general corrosion although alternative measurements of corrosion rate by coupon immersion testing, electrochemical impedance spectroscopy, or polarization resistance methods are suggested to confirm predictions since corrosion rates cannot be easily estimated from polarization scans. Localized corrosion in the form of crevice corrosion or pitting is not suggested. An activation peak was seen during the forward scan at a current density Ia of 3.17 μA and a reactivation peak at a current density Ir of 1.04 μA giving a ratio of Ir/Ia of 0.33 showing some suspicion of probable activity at the grain boundaries.

The sample that was sensitized at 750 C for about 6000 minutes predicted that, risk of localized corrosion in the form of crevice corrosion is present. Such areas as close proximity of surfaces, areas under deposits, and metal-Silicone-O-ring interfaces may be prone to such attack. Pitting may be observed in non-occluded areas. Longer term immersion tests with, for example, artificial crevice formers, are implied to confirm prediction. No general corrosion was predicted in this sample. An activation peak was seen during the forward scan at a current density Ia of 6.8 A and a reactivation peak at a current density Ir of 2.8 μA giving a ratio of Ir/Ia of 0.41 showing some suspicion of probable activity at the grain boundaries.

In the solutionized samples, the one that was solutionized at 1150C for 30 minutes showed extremely low risk of localized corrosion and no general corrosion was predicted., the one that was solutionized at 1125C for 30 minutes also showed extremely low risk of localized corrosion and no general corrosion was predicted, and the one solutionized at 1175 C for 120 minutes showed predictions of general corrosion, although alternative measurements of corrosion rate, like coupon immersion testing, electrochemical impedance spectroscopy, or polarization resistance methods are suggested to confirm predictions since corrosion rates cannot be easily estimated from polarization scans. Localized corrosion in the form of crevice corrosion or pitting is not suggested.

Double-Loop EPR Tests for Cr Depletion

The samples that were tested included a mill-annealed sample, sensitized sample at 750 C for 600 minutes, sample sensitized at 750C for 6000 minutes, batch-2 sample sensitized at 700C for 6000 minutes, and a sample solutionized at 1175C for 120 minutes. All of them showed that localized corrosion in the form of crevice corrosion or pitting is not suggested although all of them showed mostly activation peaks in the forward direction. Some amount of general corrosion was suspected but alternative measurements of corrosion rate by coupon immersion testing, electrochemical impedance spectroscopy, or polarization resistance methods are suggested to confirm predictions since corrosion rates cannot be easily estimated using polarization scans.

The mill-annealed sample showed an activation peak at a current density of 9.173 μA, sensitized sample at 750 C for 600 minutes showed an activation peak at a current density of 40.08 μA, sample sensitized at 750C for 6000 minutes showed an activation peak at a

current density of 62.12 μA, batch-2 sample sensitized at 700C for 6000 minutes showed an activation peak at a current density of 13.7 μA, and a sample solutionized at 1175C for 120 minutes showed an activation peak at a current density of 181.1 μA.

Double-Loop EPR Tests for Mo Depletion

The samples that were tested included a mill-annealed sample, batch-2 sample sensitized at 700 °C. for 6000 minutes. All of them showed that localized corrosion in the form of crevice corrosion or pitting is not suggested although all of them showed mostly activation peaks in the forward direction. Some amount of general corrosion was suspected but alternative measurements of corrosion rate by coupon immersion testing, electrochemical impedance spectroscopy, or polarization resistance methods are suggested to confirm predictions since corrosion rates cannot be easily estimated using polarization scans.

The mill-annealed sample showed an activation peak at a current density of 18.93 μA.

Conclusions of Subtask 2

The results of the ASTM-G-28 chemical weight loss tests were analyzed and plotted so as to obtain a broader understanding of the various correlations between the parameters like heat treatment times, temperatures and sources of the raw metal obtained in the mill annealed condition. The samples in the mill-annealed condition showed corrosion rates ranging from 5.11 mpy to 29.52 mpy for different samples after the ASTM-G-28-A test. The ASTM-G-28-B test results showed corrosion rates ranging from 3.96 mpy to 26.55 mpy for various mill-annealed Alloy-22 samples. There was also a clear effect of the time of sensitization on the corrosion rate with the average corrosion rate of the various samples done for every segment of the time of sensitization clearly increasing in the direction of the larger times of sensitization. There was again the relevance of increase in the temperature of sensitization on the corrosion rates. In general the average corrosion rates of sensitized samples of Alloy 22 were about 100 times higher for the ASTM-G-28-B test compared to the ASTM-G-28-A tests. The solution heat treatment showed corrosion rates that peaked at lower temperatures for higher times of heat treatment compared to the sensitization treatment that showed corrosion rates which peaked at both higher temperatures and times of sensitizations. The maximum corrosion rates though were the highest in sensitized samples and the average corrosion rate was also higher in sensitized samples. The tests results indicated that the samples are more vulnerable to higher intergranular corrosion as influenced by variations in the parameters for processing. The samples in general exhibited higher corrosion rates in ASTM G-28-B tests.

The double-loop EPR (Electrochemical Potentiokinetic Reactivation) test results showed that all the mill-annealed samples in the various test conditions showed that the risk of localized corrosion is extremely low. Even the general corrosion is not predicted, the general corrosion rate may be at most a contamination rate. One mill-annealed sample showed suspected risk of localized corrosion in the acidic condition that is a form of crevice corrosion which might be present in areas such as close proximity of surfaces, areas under deposits, and metal- silicone O-ring interfaces may be prone to such attack. But such assumptions can only be conformed using longer term immersion tests with, for example, artificial crevice

formers which are implied to confirm crevice corrosion prediction. In the basic condition though general corrosion is not predicted, in one of the samples, there is a suspected general corrosion rate that may be predicted to be measurable. Alternative measurements of corrosion rate like coupon immersion testing, electrochemical impedance spectroscopy, or polarization resistance methods are suggested to confirm these predictions since corrosion rates cannot be easily estimated from polarization scans.

Most of the sensitized samples showed that no attack is being predicted. The risk of localized corrosion was extremely low so as to call it negligible. Even general corrosion was not predicted at all in these samples. Some sensitized samples which were sensitized for longer periods and higher temperatures showed that the risk of localized corrosion in the form of crevice corrosion in close proximity of surfaces such as metal-O-ring interfaces etc. might be there. Though longer term immersion tests with, for example, artificial crevice formers are implied to confirm crevice corrosion prediction.

Most of the solutionized samples showed that no attack is being predicted. The risk of localized corrosion was extremely low so as to call it negligible. Even general corrosion was not predicted at all in these samples. Some solutionized samples that were solutionized for longer periods and higher temperatures showed that the risk of localized corrosion in the form of crevice corrosion in close proximity of surfaces such as metal-O-ring interfaces etc. might be there. Though longer term immersion tests with, for example, artificial crevice formers are implied to confirm crevice corrosion prediction.

Very few of them showed suspected measurable general corrosion rate. This needs to be substantiated using alternative measurements of corrosion rate by coupon immersion testing, electrochemical impedance spectroscopy, or polarization resistance methods which are used to confirm predictions.

All the samples that were tested for Cr- depletion, Mo-Depletion showed that localized corrosion in the form of crevice corrosion or pitting is not suggested although all of them showed mostly activation peaks in the forward direction. Some amount of general corrosion was suspected but alternative measurements of corrosion rate by coupon immersion testing, electrochemical impedance spectroscopy, or polarization resistance methods are suggested to confirm predictions since corrosion rates cannot be easily estimated using polarization scans. The ASTM-G-28 Tests are carried out in highly exaggerated conditions that the material may not face in the actual repository condition. Although it did show that there was effect of the processing parameters on the material in its sustained endurance to face corrosion at these exaggerated conditions. This can be used as an input to look for the exact behavior of Alloy-22 at the exact repository conditions after going through various processes like welding, brazing etc. The Double-Loop EPR tests showed that the material was very resistant to localized corrosion in conditions that contained high amounts of chloride conditions and even the Chromium and Molybdenum depletion wasnt present in higher quantities that could lead to intense localized corrosion. The sensitization at the grain boundaries was minimal as no prominent activation/reactivation peaks were found in almost all the samples. The very minimal activity that was present at the grain boundaries was more in the sample that was sensitized at higher temperatures like 750 C for higher periods like 6000 minutes in highly acidic and basic chloride solutions. A stray case of sensitization was seen in one of the solutionized sample. Although these results need to be substantiated

using alternative methods like longer term immersion tests with, for example, artificial crevice formers, coupon immersion testing, electrochemical impedance spectroscopy, or polarization resistance methods etc at the exact repository conditions.

Subtask 3: Diffusion

Goals

The diffusion studies were conducted as non–QA scoping work to complement the other activities. This was not (technically) listed as a subtask in the original SIP (only as scoping work). The goals of this study were as follows.

1. Measure the diffusivity matrix of the ternary equivalent of Alloy–22 at metallurgical temperatures near the solutionizing temperature of the alloy.

2. Develop an understanding of what will be necessary in order to determine the diffusivity of this alloy at repository operating conditions. I.e., examine the feasibility of low–temperature measurements.

3. Develop an understanding of the roles of experimental uncertainties in long–term diffusion measurements (i.e., at low temperature).

This study was centered on experimental measurements, but involved a considerable amount of theoretical work in order to properly understand the data and the feasibility of future low–tempearture studies.

To most efficiently gather and analyze the diffusion couple data, a regression scheme was developed in–house, which combined both heuristic and nonlinear regression components to provide a combination of efficient operation with accurate results.`This regresssion scheme` has been published in [24]. The scheme is outlined in Figure 9.

Results of Subtask 3

Validation of Regression Methods

The regression method was tested in order to know how well it can reproduce the original diffusivity matrix $[D]$. Validation was done using simulated concentration profiles generated according to expressions from an hypothetical diffusivity matrix.

The element analysis techniques, like EPMA, used here, have an intrinsic uncertainty leading to errors in the measured value. Therefore, in order to know how the method will behave considering data scattering, artificial noise was included in the original data in order to know how the calculated value for $[D]$ varies when compared with the original. The end compositions for the simulated diffusion couples are presented in Table 2.The different cases evaluated are described below. All cases were simulated for "$t = 200h$". The results for the calculated diffusivity matrix and the square root diffusivity matrix are presented in Tables 3 and 4 respectively. Table 5 shows the results for the eigenvalues of the diffusivity matrix and

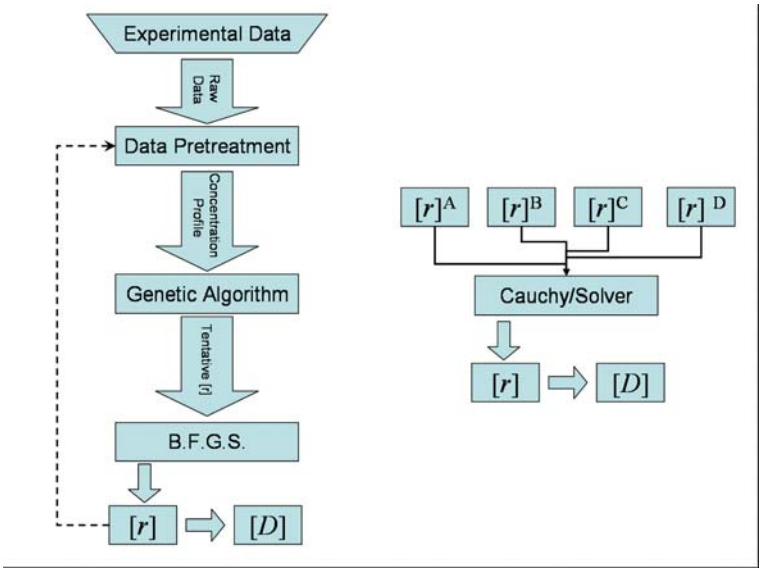

Figure 9: Flow chart representation of regression strategy

the square root diffusivity matrix. The effectiveness of the regression scheme is illustrated using simulated diffusion couple data in Figure 10.

- Original: Starting values for $[D]$, corresponding to an hypotetical system.
- Case I : The simulated experimental data is considered without noise.
- Case II : The simulated experimental data is considered with noise given by $C_i = C_i^c \pm 1.0at\%$
- Case III: The simulated experimental data is considered with noise given by $C_i = (1 \pm 2.0\%)\ C_i^c$

MonteCarlo simulations

MonteCarlo simulations for the error in the measurement considering a flat distribution were done. The values of the original diffusivity matrix $[D]$, diffusion couples and time are the same that the used in the previous section.

The data was statistically analyzed for the diffusivity matrix $[D]$. In addition, the statistical analysis for the diffusivity matrix eigenvalues E_1, E_2 are included. In the tables 6, 7, 8 and 9 there are presented the results for the different uncertainty levels.

In the figure 11 there is presented graphically the dependence between the uncertainty in the concentration value and their effect in the uncertainty in the diffusivity matrix.

Table 2: End compositions for simulated experimental data, in %at

	Couple # 1		Couple # 2	
	C_i^-	C_i^+	C_i^-	C_i^+
Element 1	30	55	25	20
Element 2	45	25	30	40
Element 3	25	20	45	40

Table 3: Diffusivity Matrix: Original and Calculated Data. All the values are in 10^{-11} $[\mathsf{cm}^2/\mathsf{s}]$

$[D]$	Original	Case I	Case II	CaseIII
D_{11}	12.1	12.1	14.8	12.6
D_{12}	5.16	5.14	7.82	5.76
D_{21}	1.74	1.74	-2.15	0.244
D_{22}	6.25	6.25	2.21	4.74

Table 4: Square Root Diffusivity Matrix: Original and Calculated Data. All the values are in 10^{-6} $[\mathsf{cm}^2/\mathsf{s}]$

$[r]$	Original	Case I	Case II	CaseIII
r_{11}	10.9	10.9	12.4	11.2
r_{12}	2.75	2.76	4.44	3.19
r_{21}	.934	0.933	-1.22	0.135
r_{22}	7.74	7.74	5.25	6.85

Table 5: Eigenvalues for the diffusivity matrix and the square root diffusivity matrix. The diffusivity matrix eigenvalues E_i are in $[\mathsf{cm}^2/\mathsf{s}]$, the square root matrix eigenvalues e_i are in $\left[\mathsf{cm}/\mathsf{s}^{1/2}\right]$

	Original	Case II	CaseIII
$E_1/10^{-11}$	13.4	13.3	12.8
$E_2/10^{-11}$	4.99	3.73	4.57

	Original	Case II	CaseIII
$e_1/10^{-6}$	11.6	11.5	11.3
$e_2/10^{-6}$	7.06	6.11	6.77

Table 6: Statistical results for uncertainty analysis for $\eta = 0.1\%$. All values are in $(10^{-11}$ $[\mathsf{cm}^2/\mathsf{s}])$

	$\eta = 0.1\%$					
	D_{11}	D_{12}	D_{21}	D_{22}	E_1	E_2
Mean	12.1	5.13	1.74	6.25	13.4	5.00
Median	12.1	5.13	1.75	6.26	13.4	5.00
Standard Deviation	.0849	.0938	.0663	.0728	.0893	.0260
Coefficient of Variation	.00700	.0183	.0381	.0117	.00668	.00520

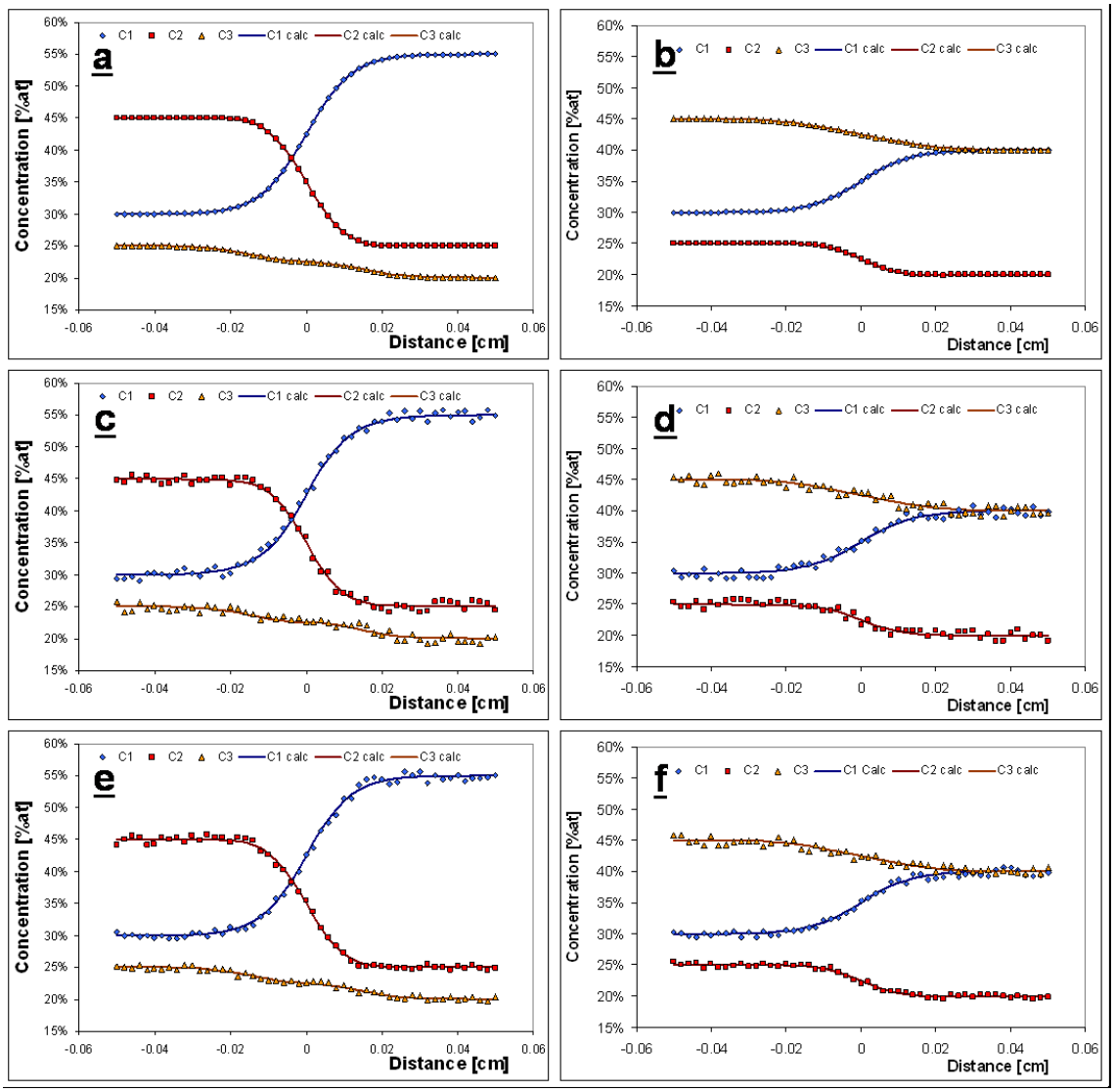

Figure 10: Concentration profiles for simulated diffusion couples, for a simulation time of 200 hours. Dots correspond to simulated data, and the continuous lines correspond to calculated data. a)Diffusion Couple #1, Case I; b) Diffusion Couple #2, Case I; c) Diffusion Couple #1, Case II; d) Diffusion Couple #2, Case II; e) Diffusion Couple #1, Case III; f) Diffusion Couple #2, Case III.

Table 7: Statistical results for uncertainty analysis for $\eta = 0.2\%$. All values are in $(10^{-11}\ [\mathsf{cm}^2/\mathsf{s}])$

	$\eta = 0.2\%$					
	D_{11}	D_{12}	D_{21}	D_{22}	E_1	E_2
Mean	12.1	5.15	1.73	6.24	13.4	4.99
Median	12.1	5.16	1.73	6.24	13.4	5.00
Standard Deviation	.154	.169	.121	.131	.158	.0463
Coefficient of Variation	.0127	.0329	.0697	.0210	.0118	.00928

Table 8: Statistical results for uncertainty analysis for $\eta = 0.5\%$. All values are in $(10^{-11}\ [\mathsf{cm}^2/\mathsf{s}])$

	$\eta = 0.5\%$					
	D_{11}	D_{12}	D_{21}	D_{22}	E_1	E_2
Mean	12.1	5.12	1.73	6.24	13.4	5.00
Median	12.1	5.10	1.76	6.27	13.3	5.01
Standard Deviation	.438	.489	.341	.372	.466	.131
Coefficient of Variation	.0361	.0954	.197	.0597	.0348	.0262

Table 9: Statistical results for uncertainty analysis for $\eta = 1.0\%$. All values are in $(10^{-11}\ [\mathsf{cm}^2/\mathsf{s}])$

	$\eta = 1.0\%$					
	D_{11}	D_{12}	D_{21}	D_{22}	E_1	E_2
Mean	12.0	4.96	1.71	6.23	13.2	5.01
Median	12.0	4.99	1.71	6.23	13.3	5.01
Standard Deviation	1.02	1.13	.649	.713	1.13	.280
Coefficient of Variation	.0853	.228	.379	.115	.0858	.0559

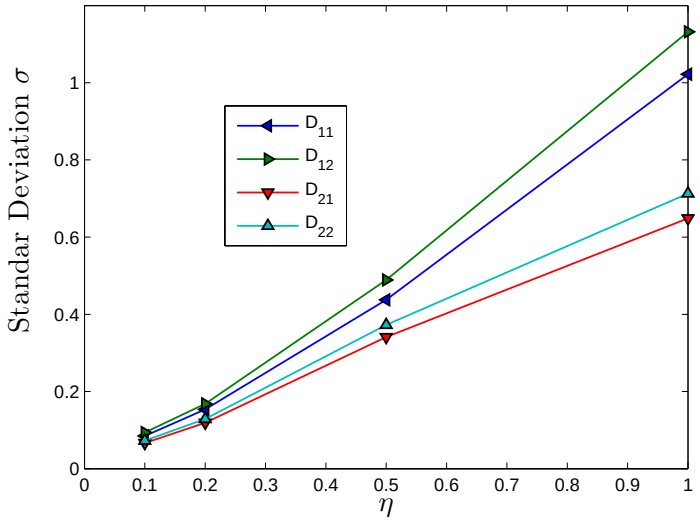

Figure 11: Standard deviation for the diffusivity matrix at different levels of uncertainty in the concentration

Role of the Instrument Error in the Diffusivity Matrix *[D]*

The estimation of *[D]* is made using experimental data. These data, in this case, corresponds to concentrations profiles for the different elements across a diffusion couple, determined using Electron Micropobe Analysis (EMPA). Considering that the measured data represent the experimental values for concentration at the exact point reported by the instrument, any discrepancies in the value of *[D]* would corresponds to the estimation method used. However experimental data is not error free and this effect would translate in a discrepancy between the real and the estimated values for *[D]*. This discrepancy could affect not only the prediction for the kinetics at the expeirments temperatures. When the results are used for temperature dependence estimations, those errors could be magnified.

Thus there is evolved the interest to quantify the effect of the errors in the experimental results in the reliability of *[D]*. Knowing those dependences, would permit also the design of cost efficients experiments by evaluating the role of the differents factors.

Here different types of the instrumental analysis errors were considered.

- Type I, Sampling Volume: In fact the EMPA does not mesure the concentration in a given value, instead it take an avarage of the composition foir a certain value.
- Type II, Spatial Positioning and Resolution: The probe positioning present an intrinsic uncertainty. It affects the reliability of that a certain experimental value correspond to a given location.
- Type III, Concentration error. As in any concentration analysis method there is an , `sometimes known`, associated presicion and sensivity for the method,

Errors type I and II are associated with the "size"' of the experimental sample. I becomes relevant when due to experimental constrains there is considered a small penetration depth.Whereas error type III becomes relevant for small concentration differences between the end compostions in the diffusion couples. Here the effects of the errors type I, II, and III were analyzed Uncertainty Quantification (UQ) using Monte Carlo simulation of error propagation through measurement and analysis procedures.

Type I error: Spot size This type of error can be described by a deterministic expression (1).

$$C_i^{Obs}(x,t) = \frac{1}{V_{Spot}} \int_{V_{Spot}} \phi(V_{Spot}) \cdot C_i^{Orig}(x,t) dV_{Spot} \tag{1}$$

Where C_i corresponds to the concentration profile of the element i, V is the analytical (sampled) volume, ϕ is the spatial variation of the sampled volume, and the superscripts $Orig$ and Obs correspons to the experimental (true) value of of the concentration and the value reported by the instrument, respectively.

Considering that there is no spatial variation in the interaction volume, the contribution to the error in *[D]* ($\delta D_{ij}, \quad i,j = 1,2$) is given by:

$$\delta D_{ii} = \alpha \cdot \frac{r_{spot}^2}{t} \tag{2}$$

Where r_{spot} is the radius of the analytical volume, t is the diffusion time and α is a proportionality constant depending on the system. The double indice ii in the uncertainty term, states that this relationship only holds for diagonal terms.

Type II error: Spatial postioning This type of error can be described by a stochastic expression (3).

$$C_i^{Obs}(x^{Obs}, t) = C_i^{Orig}(x^{Orig}, t) \quad \Rightarrow \quad \left(x^{Obs} - x^{Orig}\right) \sim N(0, \sigma_x^2) \tag{3}$$

In other words the difference between the original and the observed position is Gaussian distributed with an variance of σ_x^2. The effect of this into the uncertainty in *[D]* was determined to be given by:

$$\frac{\sigma_{D_{ij}}}{D_i j} \propto \frac{\sigma_x}{\sqrt{n_{points}}} \frac{1}{t^m} = const. \tag{4}$$

Where $\sigma_{D_{ij}}$ is the uncertainty in the diffusivity matrix *[D]*,n_{points} is number of experimental measurements (uniformly distributed) across the diffusion couples and m is an exponent depending of the system. Also it was found that the normalized uncertainty (right hand side of the previous equation) is constant for all terms in *[D]*. This expression allows a fast estimation fo the effect of incrementing the number of data point in the uncertaint of *[D]*.

Type III error: Spatial postioning This type of error can be described by a stochastic expression (5).

$$C_i^{Obs}(x, t) = C_i^{Orig}(x, t) + \delta C \quad \Rightarrow \quad \left(C_i^{Obs} - C_i^{Orig}\right) \sim N(0, \sigma_{C_i}^2) \tag{5}$$

In other words the difference between the original and the observed concentration is Gaussian distributed with an variance of $\sigma_{C_i}^2$. The effect of this into the uncertainty in *[D]* was determined to be given by:

$$\frac{\sigma_{D_{ij}}}{D_i j} \propto \frac{\sigma_{C_i}}{C_i} \tag{6}$$

Thus the normalized uncertainty in the diffusivity matrix is proportional to the normalized uncertainty in the concentration. Since the the uncertainty in the concentration depends on the time used for detection in EMPA, this expression allows a quick estimation of the effect of increment the analysis time in the reduction of the uncertianty on *[D]*.

Diffusivity of Ni–Cr–Mo Alloy–22 Analog

Four diffusion couples made from the alloys listed in the table 10 were produced.

The starting alloys are listed below:

- Couple I : Alloys #1 & #2.

Table 10: Alloys composition in % wt

Alloy#	Weight %		
	Ni	Cr	Mo
1	66.0	20.2	14.0
2	72.1	15.1	12.8
3	67.7	15.7	16.6
4	72.9	17.4	9.7
5	69.7	21.2	9.1
6	64.3	24.3	11.4

- Couple II : Alloys #1 & #3.
- Couple III: Alloys #1 & #4.
- Couple IV: Alloys #1 & #2.

The diffusion couples were annealed for 48 hours at 1215 ± 5 °C.

From each diffusion couple, two EPMA line scans were produced. In the tables 11, 12, 13, and 14, are presented the measured composition from each line scan.

Since the method implemented here to find the diffusivity matrix $[D]$ requires the concentration profile for two diffusion couples, the data obtained was grouped in the following cases:

- Case A: Couple I, Line scan #1; & Couple II, Line scan #1.
- Case B: Couple I, Line scan #2; & Couple II, Line scan #2.
- Case C: Couple IV, Line scan #1; & Couple III, Line scan #1.
- Case D: Couple IV, Line scan #2; & Couple III, Line scan #2.

The diffusivity and the square root diffusivity matrix and their eigenvalues considering Mo as base element were determined from each case. The results, including the eigenvalues for the matrices, are presented in the tables 15 and 16.

Table 11: End compositions for diffusion couples I, in %at

	Couple I			
	Line scan # 1		Line scan # 2	
	C_i^-	C_i^+	C_i^-	C_i^+
Nickel	67.0	73.3	67.1	73.3
Chromium	24.6	18.6	24.7	18.6
Molybdenum	8.3	8.0	8.3	8.0

Table 12: End compositions for diffusion couples II, in %at

	Couple II			
	Line scan # 1		Line scan # 2	
	C_i^-	C_i^+	C_i^-	C_i^+
Nickel	67.1	70.0	67.0	69.9
Chromium	24.7	19.8	24.7	19.8
Molybdenum	8.2	10.2	8.2	10.2

Table 13: End compositions for diffusion couples III, in %at

	Couple III			
	Line scan # 1		Line scan # 2	
	C_i^-	C_i^+	C_i^-	C_i^+
Nickel	68.1	74.0	68.1	74.0
Chromium	23.8	20.4	23.9	20.4
Molybdenum	8.1	5.6	8.1	5.6

Table 14: End compositions for diffusion couples IV, in %at

	Couple IV			
	Line scan # 1		Line scan # 2	
	C_i^-	C_i^+	C_i^-	C_i^+
Nickel	68.0	74.1	68.0	74.2
Chromium	23.8	18.0	23.9	17.9
Molybdenum	8.2	7.9	8.2	7.9

Table 15: Diffusivity Matrix: Diffusion Couples at 1215 °C. All the values are in 10^{-10} [cm^2/s]

$[D]$	Case A	Case B	Case C	CaseD
D^{Mo}_{NiNi}	4.26	3.84	5.68	4.37
D^{Mo}_{NiCr}	0.228	0.199	1.96	0.382
D^{Mo}_{CrNi}	-1.64	-1.181	-2.82	-1.95
D^{Mo}_{CrCr}	2.05	2.20	0.485	1.59
E_1	4.08	3.68	4.18	4.07
E_2	2.23	2.36	1.98	1.89

Table 16: Sq. Root Diffusivity Matrix: Diffusion Couples at 1215 °C. All the values are in 10^{-5} $[\mathsf{cm}^2/\mathsf{s}]$

$[r]$	Case A	Case B	Case C	CaseD
r^{Mo}_{NiNi}	2.07	1.96	2.48	2.10
r^{Mo}_{NiCr}	.0650	.0576	.568	.113
r^{Mo}_{CrNi}	-.466	-.342	-.817	-.576
r^{Mo}_{CrCr}	1.44	1.49	0.975	1.29
e_1	2.02	1.92	2.04	2.02
e_2	1.49	1.54	1.41	1.37

From the previous results, we obtained the average for the elements in the square root diffusivity matrix. This value was used as the starting point for the global fitting. The diffusivity matrix and the square diffusivity matrix obtained from the global fitting are presented below for the different elements (Mo, Ni, Cr) as base element.

$$\begin{bmatrix} D^{Mo}_{NiNi} & D^{Mo}_{NiCr} \\ D^{Mo}_{CrNi} & D^{Mo}_{CrCr} \end{bmatrix} = \begin{bmatrix} 4.60 & 0.681 \\ -1.87 & 1.70 \end{bmatrix} \cdot 10^{-10} \left[\mathsf{cm}^2/\mathsf{s}\right]$$

$$\begin{bmatrix} D^{Ni}_{CrCr} & D^{Ni}_{CrMo} \\ D^{Ni}_{MoCr} & D^{Ni}_{MoMo} \end{bmatrix} = \begin{bmatrix} 3.57 & 1.87 \\ 0.349 & 2.73 \end{bmatrix} \cdot 10^{-10} \left[\mathsf{cm}^2/\mathsf{s}\right]$$

$$\begin{bmatrix} D^{Cr}_{MoMo} & D^{Cr}_{MoNi} \\ D^{Cr}_{NiMo} & D^{Cr}_{NiNi} \end{bmatrix} = \begin{bmatrix} 2.38 & -0.349 \\ -0.680 & 2.73 \end{bmatrix} \cdot 10^{-10} \left[\mathsf{cm}^2/\mathsf{s}\right]$$

$$\begin{bmatrix} r^{Mo}_{NiNi} & r^{Mo}_{NiCr} \\ r^{Mo}_{CrNi} & r^{Mo}_{CrCr} \end{bmatrix} = \begin{bmatrix} 2.17 & 0.194 \\ -0.533 & 1.34 \end{bmatrix} \cdot 10^{-5} \left[\mathsf{cm}/\sqrt{\mathsf{s}}\right]$$

$$\begin{bmatrix} r^{Ni}_{CrCr} & r^{Ni}_{CrMo} \\ r^{Ni}_{MoCr} & r^{Ni}_{MoMo} \end{bmatrix} = \begin{bmatrix} 1.88 & 0.533 \\ 0.0993 & 1.64 \end{bmatrix} \cdot 10^{-5} \left[\mathsf{cm}/\sqrt{\mathsf{s}}\right]$$

$$\begin{bmatrix} r^{Cr}_{MoMo} & r^{Cr}_{MoNi} \\ r^{Cr}_{NiMo} & r^{Cr}_{NiNi} \end{bmatrix} = \begin{bmatrix} 1.54 & -0.0993 \\ -0.194 & 1.98 \end{bmatrix} \cdot 10^{-5} \left[\mathsf{cm}/\sqrt{\mathsf{s}}\right]$$

The results presented above were used with the end compositions to generate the calculated concentration profile for each case. The experimental and calculated concentration profiles are presented in Figures 12 and 13. In addition, the experimental and calculated diffusion profile for all cases in the composition space (Cr,Mo at%) are shown in figure 14 .

As additional comment, in the EPMA analysis of the diffusion couples no porosity was observed, neither in the original interface or the bulk of the diffusion couple. The imaging in this equipment was generated from secondary electrons with a magnification of 125 X (approx.).

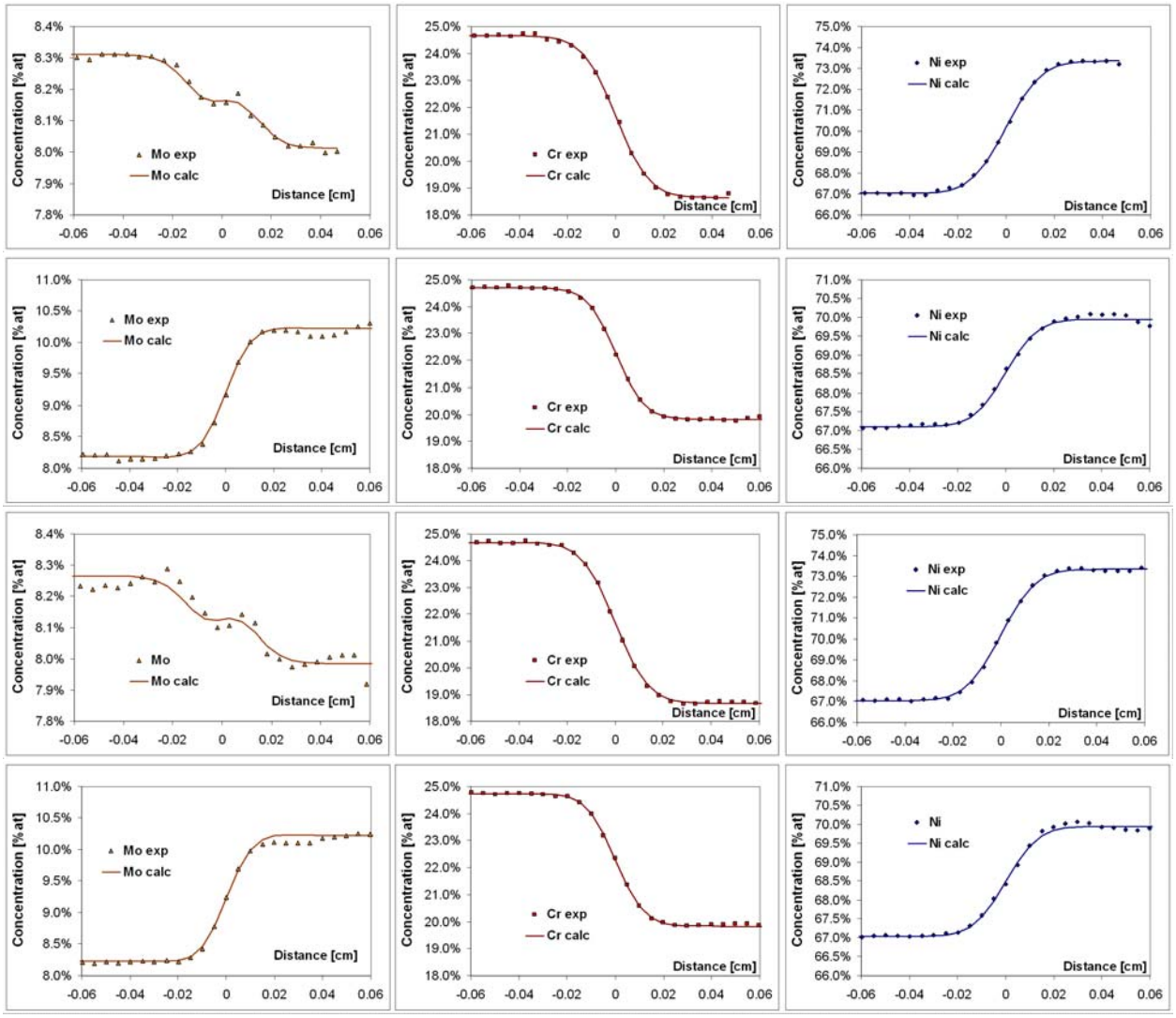

Figure 12: Calculated and experimental concentration profiles for Molybdenum (Right), Chromium (Center) and Nickel (Left). Presented are the results for the interval $\pm 0.06\,[\mathsf{cm}^2]$ from the initial interface in order to show in more detail the *penetration* zone of the diffusion front. *First Row*: Couple I, Line scan #1; *Second Row*: Couple II, Line scan #1; *Third Row*: Couple I, Line scan #2; *Fourth Row*: Couple II, Line scan #2.

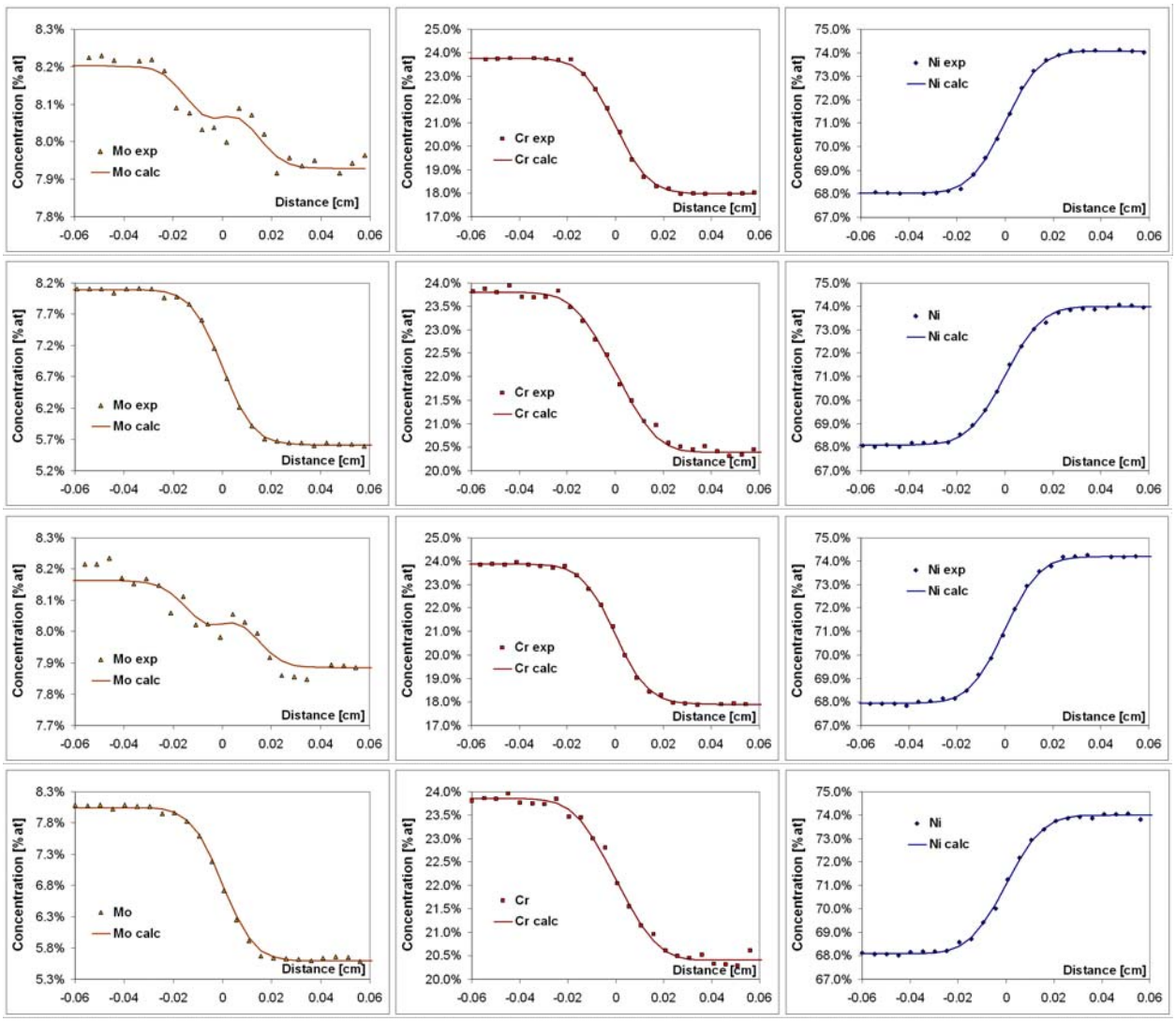

Figure 13: Calculated and experimental concentration profiles for Molybdenum (Right), Chromium (Center) and Nickel (Left). Presented are the results for the interval $\pm 0.06\,[\mathsf{cm}^2]$ from the initial interface in order to show in more detail the *penetration* zone of the diffusion front. *First Row*: Couple IV, Line scan #1; *Second Row*: Couple III, Line scan #1; *Third Row*: Couple IV, Line scan #2; *Fourth Row*: Couple III, Line scan #2.

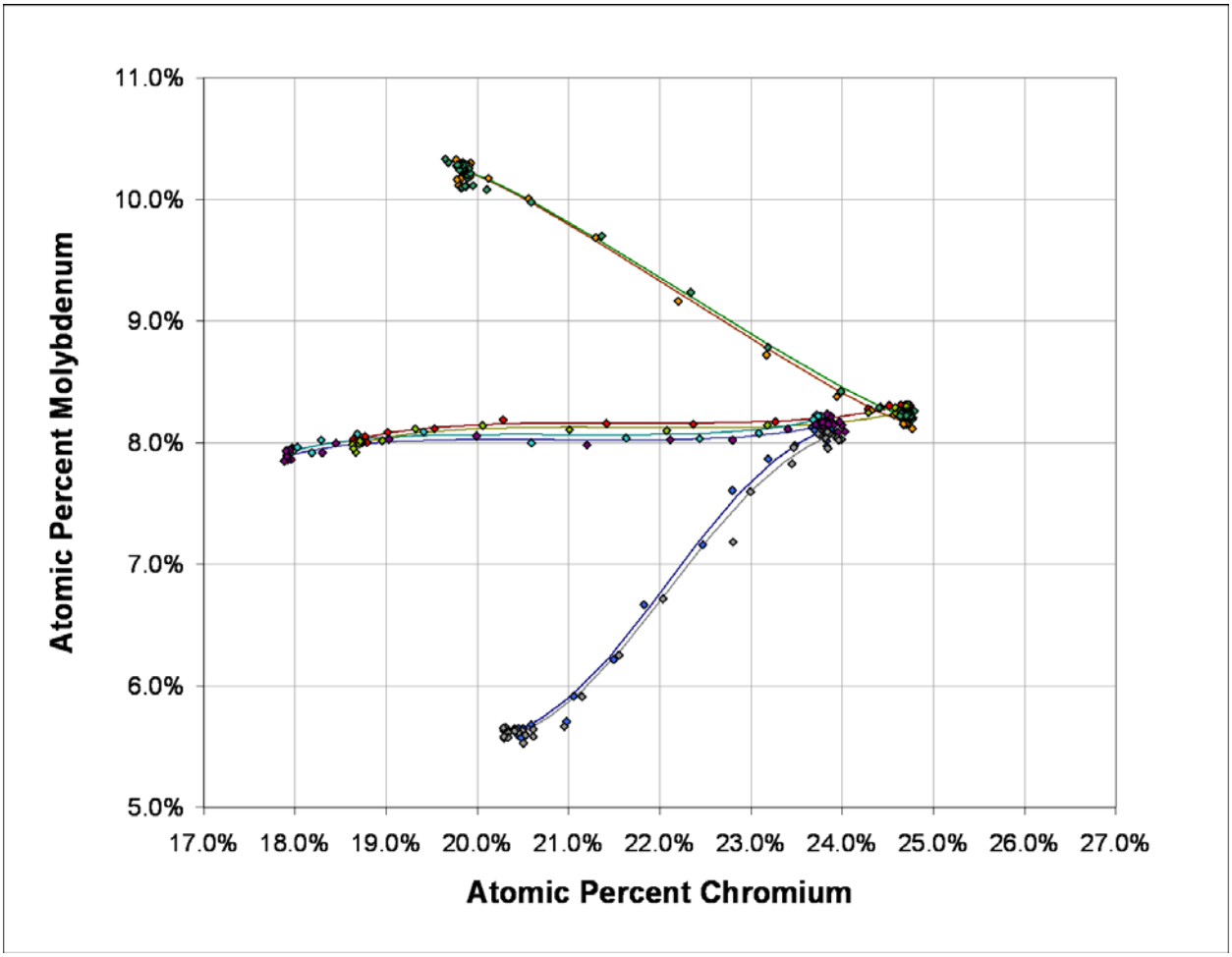

Figure 14: Diffusion profiles in the composition space. All the concentration profiles, experimental (dots) and calculated (continuous line), are shown here. The difference between the end compositions from each case can be associated to the segregation in the starting alloy.

Conclusions of Subtask 3

Simulated Data

The analysis using simulated data allow for checking fast and qualitatively the degree of fitness of the calculated diffusivity matrix obtained through the method presented here. The results case I (without noise) show an excellent agreement with the original diffusivity matrix, being that the values are practically identical. No method in the literature was able to get a lower error in a test comparing original and calculated diffusivity matrix. However, the method presented here requires the results for two diffusion couples.

Using the method implemented here it was possible to generate a set of results from data with a certain degree of scattering. The data obtained in the cases II and III show less agreement with the original diffusivity matrix, but the calculated and original concentration profiles shows a good agreement. That implies an improvement compared with the previous

methods, since most of them require smooth concentration profiles.

The agreement between the original and calculated data for the cases II and III can be confirmed analyzing the eigenvalues for the calculated diffusivity matrix.

From the analytical solution for the diffusion equation the eigenvalues of the square root diffusivity matrix defines the penetration depth of the diffusion process. Therefore, comparing the eigenvalues could give an idea of how close are the estimated penetration and general shape for the diffusion profile. It confirms that although some of the terms in the calculated diffusivity matrix differ from the original, the calculated diffusivity matrix is still able to represent the diffusion phenomena. The maximum difference between the square root diffusivity matrix eigenvalues are 14% for Case II and 4% for Case III.

One way to reduce the deviation is to use a high number of experimental data, or more diffusion couples. In the case that the method implemented here is reliable, it is expected that the error propagation must decrease with the reduction in the scattering of the original data. The analysis using MonteCarlo simulations confirms those statements.

Monte Carlo Simulations

The analysis done using MonteCarlo simulations can be seen as an extension of the result presented in the previous section. Considering a large number of simulations allows for generalizing the conclusions and reducing the impact of particular results. These results were generated using an uniform probability distribution for the error in the concentration value. If a direct representation of the error effect from a specific instrument is required, the use of a proper probability distribution will lead to more representative results.

The values of the mean and the median are almost coincident enabling to state that the skewness for the data distribution can be neglected. It allows for considering the mean as representative value for the data, and it is a required condition to consider that the values follow a Gaussian distribution. The symmetry on the data distribution and their closeness of the mean for each data set to the original values support that an extensive analysis using duplicate data would converge in a good approximation to the real value of diffusivity matrix.

An interesting result can be observed in the values of the coefficient of variation ($s/\overline{x}$). There is an inverse relationship between the value of the terms in the diffusivity matrix (D_{ij}) and its coefficient of variation. In other words, the smallest values in the diffusivity matrix will show a higher range of uncertainty. So, the highest value in the diffusivity matrix is better estimated than the rest of the values.

The eigenvalues show a different behavior, the smallest eigenvalues show a lower coefficient of variance than the highest one. In addition, the coefficient of variance is ever lower for the eigenvalues than the ones for the terms in the diffusivity matrix. Considering that the eigenvalues define the penetration depth and the error in the position is negligible, the estimation on the penetration depth is done efficiently.

From the figure 11 it is possible to see that value of the standard deviation goes to zero as the value of the uncertainty in the measured concentration profiles goes to zero. Although those results are only directly applied to the simulated cases, it is possible to analyze how the reliability of the results is affected as the error in the concentration analysis is increased. Since the experimental results presented here are obtained with an uncertainty

in the composition analysis around 1% (for Molybdenum), there it is no guarantee that a good value is obtained for the diffusivity matrix using the results of only two diffusion couples.

The standard deviation shows a dependence which can be assumed proportional for the range analyzed. This helps to analyze how the reduction in the error on the analysis will affect the uncertainty in the results. As an example in the case of EPMA analysis the error could be approximated as the square of the analysis time, since the counting in the instrument can be associated to a Γ distribution. Therefore, if it is required to reduce the uncertainty in calculated diffusivity matrix by half, it will be required to increment the analysis time four times.

Diffusion Couple Results

Most of the concentration profiles measured show a smooth "s" shaped curve. Nevertheless the results for Molybdenum in the Couples I & IV show a high degree of scattering, making it difficult to identify a concentration profile. It can be explained considering that for those alloys there is a difference less than 0.5% between the Molybdenum end compositions, so the effects of the uncertainty in the composition analysis becomes quite relevant.

The differences between the end compositions between the lines scans (less than 0.1% at) for each diffusion couple can be explained considering the uncertainty in the EMPA analysis. However, the difference for the end compositions (alloy #1 and #2) in the couples I and II compared with the end compositions for the couples III and IV are much more relevant, being about 1% of difference (section 14). This effect can be explained from the axial segregation in the original alloy. Since wafers for the diffusion couples are obtained from the same slug and the alloys was poured in a cylindrical mold, the solute rejection can produce a concentration profile like the observed here.

The data obtained for the diffusivity matrix from each case (pair of diffusion couples) shows it to be quite close between them, with the exception of the case C. In any case, the calculated values for $[D]$ are close in order of magnitude to the rest of the results. In order to consider the results for case C, as an outliner there it is needed to conduct a statistical evaluation. It will require additional data points for the diffusion couples or reproduction of the experimental diffusion couples. The diffusion couples used in case C are the same as in case D, but using different line scans, and both generate relatively different results for the diffusivity matrix.

This fact supports that the results for the terms of the diffusivity matrix are affected by the error in the concentration analysis. On the other hand, the values for the square root diffusivity matrix eigenvalues show a good agreement between each case. It confirms that although the case C produces different results it has the same penetration depth and curve shape as the case D.

In order to answer how a result for $[D]$ with a difference of an order of magnitude for some of the terms whem compared to the rest of the results could generate similar diffusion profiles, it is possible to look in detail at the computation of the eigenvalues. From the diffusional analysis theory is possible to see that the eigenvalues are more influenced by the diagonals than the non-diagonals terms in the diffusivity matrix. In addition, the eigenval-

ues are more influenced by terms with higher order of magnitude. Both effects combined allow for dietermining the highest diagonal term in the diffusivity matrix as controlling the uncertainty in the eigenvalues. Also, the impact of the lack of quality in the terms with lower order of magnitude and non diagonal in the prediction of the eigenvalues is reduced. Those observations are confirmed by the results of the case C.

From the results for cases A, B, C, D, there is obtained a global estimate value for the diffusivity matrix using the whole set of data. The degree of representation of those data can be appreciate in the figures 12 and 13. The calculated values (continuous lines) show a good agreement with the experimental data (symbols). For the results of Molybdenum in the Couples I & IV the calculated profile shows a *step* in the diffusion profile, corresponding to a near zero gradient zone in the concentration profile. Some agreement can be observed from the experimental data. Since it corresponds to a non downhill diffusion case, experimental data in previous research also show high scattering in the concentration profile in those cases [25]. Currently, there is no physical explanation for this behavior in multicomponent diffusion besides that the error in the instrument could affect the perception of particular features. In the present case it is made worse considering the low difference in the end compositions.

The zero gradient characteristic in the concentration profile for Mo in the Couples I & IV could be confirmed analyzing the angle ϕ in the space composition for this diffusion couple [26, 27]. Reporting the values for a different base element allows for direct calculation of the particularities for the system. As an example, it is possible to calculate the composition angle ϕ defined by end compositions. In order to produce a zero gradient concentration profile (ZG) [26]. Calculating it directly from Cr based square root diffusivity matrix:

$$\phi^{ZG} = \tan^{-1}\left(\frac{r^{Cr}_{NiNi}}{r^{Cr}_{MoNi}}\right) = 92.9^{\circ}$$

For comparison purposes, the composition angle ϕ for the Mo profile in the couple IV first line scan is calculated:

$$\phi^{IV} = \tan^{-1}\left(\frac{\Delta C_{Ni}}{\Delta C_{Mo}}\right) = \tan^{-1}\left(\frac{-6.1}{0.3}\right) = 92.8^{\circ}$$

The values for both angles are almost the same, confirming that for the couple IV a close to zero gradient concentration profile must be expected. This characteristic is confirmed from the concentration profile plots in the figures 12 and 13 showing this detail.

The interval of compositions analyzed in the diffusion couples are in the γ phase of the Ni-Cr-Mo system. But, it is required to note that these results do not explore the whole range of compositions for the γ phase. However, it is possible to consider that for the range of composition analyzed the calculated diffusivity matrix is representative for the problem.

Since no porosity was observed at the secondary electron image, it is expected that the Kirkendall porosity is not produced in this system. In any case, further observations using scanning electron microscopy are required to confirm this fact. In the case that no Kirkendall porosity is produced in the system, it will confirm that the changes in the molar volume through the range of compositions in the diffusion couples are negligible. It is one of the requirements that allow to use of constant diffusivities to represent the multicomponent diffusion.

General Subtask Conclusions

The inverse problem of finding the diffusivity matrix from experimental data was approached using fitting parameters combined with the analytical results for the diffusion equations. This approach was able to obtain a representative diffusivity matrix from experimental results including data scattering representing the error in the concentration analysis. The use of advance optimization strategies were a suitable technique for the non linear regression presented here. Although the method developed here was applied to a specific system, it can be applied to any system were the diffusivity matrix is expected to be approximately constant and no relevant thermodynamics effects occurs.

The effect of the error in the experimental data affects directly the uncertainty of the calculated value for the diffusivity matrix. However although the values for the terms of the diffusivity matrix D_{ij} can vary in a range from each set of data, the values of the diffusivity matrix eigenvalues tend to be more invariant. It implies that the estimation of the penetration depth in a multicomponent diffusion can be done with a fair level of uncertainty.

The use of MonteCarlo simulations to evaluate the effects of the uncertainty reveals a suitable tool for this problem. It not only allows to estimate the uncertainty in the obtained value. Also it can be used for the estimation of the impact in improvement of the quality analysis (reduction of the error) in the level of confidence in the result obtained for the diffusivity matrix.

The multicomponent diffusion in Ni-Mo-Cr for the interval of composition analyzed is effectively represented by constant diffusion coefficients. Although it is possible to shift the element base for $[D]$ through mathematical transformations, it is useful to report them for different base elements. Here having the results for different base elements it allows the direct computation of the composition angle φ required to obtain the zero gradient concentration profile for system with a constant diffusion coefficients. Therefore there is not a direct advantage in selecting the component with the higher concentration as base element, which is done traditionally in the literature.

Personnel

This cooperative agreement activity directly supported numerous personnel, serving in various roles. A list of participating personnel is below.

1 J.C. LaCombe (PI)

2 L.G. McMillion (Co-PI)

3 S. Namjoshi (Co-Pi)

4 M.E. LaCombe (Staff)

5 A. Manavbasi (Graduate Student)

6 A. Jaques (Graduate Student)

7 G. Larios (Graduate Student)

8 S. Vadwalas (Graduate Student)

Dissemination

This activity has directly led to numerous technical publications and presentations by the Principal Investigator and the numerous students supported by the grant. Several additional pubications are currently being drafted for publication in the coming year. These are listed below.

Publications:

1 *Variational Approach to the Boltzmann Mantano Methods for Determination of the Diffusivity Coefficient* IN PREPARATION FOR 2009 SUBMISSION

2 *Assessment of Ternary Multicomponent Diffusion in Alloy 22 (Ni-Cr-Mo),* Defect and Diffusion Forum, 266, 181-190 (2007) [A.V. Jaques, and J.C. LaCombe].

3 *Variation in Susceptibility of Alloy-22 to Localized Corrosion, after Various Heat Treatments,* NACE 2007 meeting, (March 2007) [S. Vadwlas, G.M. Larios, M. Taylor, A. Manavbasi, A. Jacques, G. Mcmillion, and J.C. LaCombe].

4 *Determination of the Diffusivity Matrix from Experimental Data in Ternary Systems,* 2006 SHPE Meeting, New Orleans, LA, (January 2006) [Alonso V. Jacques and Jeffrey C. LaCombe].

5 *Effect of Phase stability and Segregation on the Corrosion properties of Alloy-22 (UNS NO6022) in Base metal and Weldments,* M.S. Thesis, The University of Nevada, Reno, (December 2007) [S. Vadwalas].

6 *Microstructural Characterization of Phase Stability and Variability in Alloy 22*, M.S. Thesis, The University of Nevada, Reno, (2007) [G. Larios].

7 *Linear multicomponent diffusion in the gamma phase in the Ni-Cr-Mo system*, M.S. Thesis, The University of Nevada, Reno, (2007) [A. Jaques].

Presentations:

1 *Instrument Error and its Propagation through Diffusion Coefficient Measurement Procedures,* MS&T 2008 (Pittsburgh, PA) (October, 2008) [J.C. LaCombe*, A.V. Jaques] INVITED.

2 *Uncertainties in Multicomponent Diffusivities and the Determination of Long-Term Diffusivities at Low Temperatures,* Diffusion Working Group Meeting (NIST, Gaithersburg, MD) (May, 2008) [J.C. LaCombe*, A.V. Jaques] INVITED.

1 *Instrument Error Propagation in the Determination of Linear Ternary Multicomponent Diffusion Coefficients*, MS&T 2007 (Detroit, MI) (September 2007) [A.V. Jacques*, and J.C. LaCombe]

2 *Variation in Susceptibility of Alloy-22 to Localized Corrosion after Various Heat Treatments,* MS&T 2007 (Detroit, MI) (September 2007) [S. Vadwlas*, G.M. Larios, M. Taylor, A. Manavbasi, A. Jacques, L.G. Mc Million, and J.C. LaCombe]

3 *Scanning electron microscopy (SEM) study of heat treated Alloy 22*, Poster, 2007 NACE Meeting (March 2007) [Shatrugna Vadwlas*, Guillermo Larios, Matt Taylor, Alp Manavbasi, Alonso Jacques, Glen Mcmillion, Jeffrey C LaCombe].

4 *Assessment of Ternary Multicomponent Diffusion in Alloy 22 (Ni-Cr-Mo),* 2007 TMS Annual Meeting, Orlando FL, (February 2007) [A.V. Jaques*, and J.C. LaCombe].

5 *Determination of Diffusivity Matrix from Experimental Data in Ternary Systems*, 2006 SHPE Meeting, New Orleans, LA, (January 2006) [Alonso V. Jacques*, and Jeffrey C. LaCombe]

Other Conclusions

A large portion of the original scope of this project was completed, despite significant budget reductions and funding delays in nearly every year of the project. For the first 3 years, the project was conducted in compliance with the NSHE quality assurance program. Most of our data was formally submitted under this program, although final work on all 3 subtasks was completed only after the project became ”non-QA”. This includes three M.S. thesis documents (Jaques, Larios, and Vadwalas).

At the closure of this activity, the key remaining thoughts on this project are below.

1 Conducting the microstructure and corrosion studies on QA certified welds became prohibitively expensive because of the loss of a QA certified weld supplier. Weld material did exist from various DOE/Bechtel sources, but these materials were not available for our use. This curtailed a good portion of our original scope of work.

2 The annual budget allocations for this project were nearly alwasys delayed and reduced from the original budget. This was a significant hurdle to making continuous progress. Funds arrived very late, necessitating unnatural spending habits (save up ahead of time) that made it difficult to plan and committ to hiring staff and students.

3 There was a significant budget cut in the first year, which was when we had intended to use equipment funds to purchase a major instrument (a backscatter detector for our SEM). This cut left us without the instrument necessary to conduct some of the microstructural characterization, reducing our initial scope of work.

4. Of the three subtasks investigated here, Subtask 3 (which was actually just scoping work), is still the **most important portion of this work** deserving future research. Subtasks 1&2 have been studied independently and conclusively by other researchers, but the diffusion work conducted here remains the only experimental work investigating the diffusive contribution to long-term phase stability of Alloy-22. Numerical models conducted by other researchers [16, 17] make key assumptions regarding the extrapolation of high-temperature diffusivity data to the lower repository temperatures. I believe that this warrants better experimental verification.

Bibliography

[1] Final Report: Waste Package Materials Performance Peer Review Panel, Submitted in response to request of USDOE, Bechtel SAIC Co. `http://www.ymp.gov/documents/peer_rev/execsum.htm`, *2002.*

[2] SUMMERS, T.S.E., WALL, M.A., KUMAR, M., MATHEWS, S.J., and REBAK, R.B. *Phase Stability and Mechanical Properties of C-22 Alloy Aged in Temperature Range 590 to 760 C for 16,000 Hours*, in *Scientific Basis for Nuclear Waste Management XXII*, Materials Research Society Symposium Proceedings Vol. 556, Materials Research Society, 1999, 916-926.

[3] SUMMERS, T.S.E., REBAK, R.B., PALMER, T.A., and CROOK, P. *Influence of Thermal Aging on the Mechanical and Corrosion Properties of GTAW welds of Alloy N06022* in *Scientific Basis for Nuclear Waste Management XXV*, Materials Research Society Symposium Proceedings, Vol. 713, Materials Research Society, 2002, 45-52.

[4] REBAK, R.B., SUMMERS, T.S.E., and CARRANZA, R.M. *Mechanical Properties, Microstructure and Corrosion Performance of C-22 Alloy Aged at 260 C to 800 C.* in *Scientific Basis for Nuclear Waste Management XXIII*, Materials Research Society Symposium Proceedings, Vol. 608, Materials Research Society, 2000, 109-114.

[5] CIESLAK, M.J., HEADLEY, T.J., and JR, A.D.R., The Welding Metallurgy of HASTELLOY Alloys C-4, C-22, and C-276. Metallurgical Transactions A, 1986. 17(A), p. 2035.

[6] CIESLAK, M.J., KNOROVSKY, G.A., HEADLEY, T.J., and A. D. ROMIG, J., The Use of New PHACOMP in Understanding the Solidification Microstructure of Nickel Base Alloy weld Metal. Metallurgical Transactions A, 1986. 17(A), p. 2107.

[7] OGBORN, J.S., OLSON, D.L., and CIESLAK, M.J., Influence of Solidification on the Microstructural Evolution of Nickel Base Weld Metal. Materials Science and Engineering, 1995. 203(A), p. 134.

[8] PAN, Y.-M., DUNN, D.S., CRAGNOLINO, G.A., and SRIDHAR, N., Grain-Boundary Chemistry and Intergranular Corrosion in alloy 825. Metallurgical Transactions A, 2000. 31(A), p. 1163.

[9] MIYATA, K. and IGARASHI, M., Effect of Ordering on Susceptibility to Hydrogen Embrittlement of a Ni-Base Superalloy. Metallurgical Transactions, 1992. 23(A), p. 953.

[10] HEUBNER, U.L., ALTPETER, E., ROCKEL, M.B., and WALLIS, E., Electrochemical Behavior and its Relation to Composition and Sensitization of NiCrMo alloys in ASTM G-28 Solution. Corrosion, 1989. 45, p. 249.

[11] RAGHAVAN, M., BERKOWITZ, B.J., and SCANLON, J.C., Metall. Transactions A, 1982. 13(A), p. 979.

[12] LOPEZ, N., CID, M., PUIGGALI, M., AZKARATE, I., and PELAYO, A., Application of Double Loop Electrochemical Potentiodynamic Reactivation Test to Austenitic and Duplex Stainless Steels. Materials Science and Engineering A, 1997. 229(A), p. 123.

[13] FANG, Z., WU, Y.S., ZHANG, L., and LI, J.Q., Application of the Modified electrochemical Potentiodynamic Reactivation Method to Evaluate Intergranular Corrosion susceptibility of Stainless Steels. Corrosion, 1998. 54, p. 339.

[14] HODGE, F.G., Effect of Aging on he Anodic Behavior of Ni-Cr-Mo alloys. Corrosion, 1973. 29, p. 375.

[15] HODGE, F.G. and KIRCHNER, R.W., Corrosion, 1976. 32, p. 332.

[16] P. E. A. Turchi, L. Kaufman and Z. K. Liu, Modeling of Ni-Cr-Mo based alloys: Part I phase stability, CALPHAD, Vol.30, 2006, 70-87.

[17] P. E. A. Turchi, L. Kaufman and Z. K. Liu, "Modeling of NiCrMo based alloys: Part II Kinetics," CALPHAD, Vol. 31, 2007,237-248

[18] Hack, H.P.1983. Crevice Corrosion Behavior of Molybdenum-Containing Stainless Steels in Seawater. Materials Performance, 22, (6), 24-30. Houston, Texas: NACE International. TIC: 245826

[19] Kenneth J. Evans, Ahmet Yilmaz, S.Daniel Day, Lana L. Wong, John C.Estill, and Raul B. Rebak Using Electrochemical Methods to Determine Alloy 22s Crevice Corrosion Repassivation Potential Research Summary, High-Radiation Nuclear Waste Disposal.

[20] Hastelloy C-22 Alloy, brochure H-2019 E (Kokomo, IN: Haynes International, 1997).

[21] R.B. Rebak, Corrosion and Environmental Degradation, Volume 2 (Weinheim, Germany: Wiley-VCH, 2000), p.69.

[22] R.B. Rebak and P.Crook, Advanced materials and Processes, 157(2) (2000), pp.37-42.

[23] D. D. Gorhe, K. S. Raja, S. A. Namjoshi et al., Electrochemical Methods to Detect Susceptibility of Ni-Cr-Mo-W Alloy 22 to Intergranular Corrosion Metallurgical & Materials Transactions A, Vol. 36A, May 2005.

[24] A.V. Jaques, and J.C. LaCombe, *Assessment of Ternary Multicomponent Diffusion in Alloy 22 (Ni-Cr-Mo)*, Defect and Diffusion Forum, 266, 181-190 (2007).

[25] M. S. Thompson, J. E. Morral and A. D. Romig, *Metallurgical Transactions A* 21A (1990) p. 2679.

[26] M. S. Thompson and J. E. Morral, *Acta Metallurgica* Vol 34, No 11 (1986) p. 2201.

[27] M. S. Thompson and J. E. Morral, *Acta Metallurgica* Vol 34, No 2 (1986) p. 339.